SPIN VALVE EFFECT IN FERROMAGNET-SUPERCONDUCTOR-FERROMAGNET SINGLE ELECTRON TRANSISTOR

A Dissertation

Presented to

The Academic Faculty

By

Armando Alonso Anaya

In Partial Fulfillment

In The Requirements for the Degree

Doctor of Philosophy in Physics

Georgia Institute of Technology

January, 2005

SPIN VALVE EFFECT IN FERROMAGNET-SUPERCONDUCTOR-FERROMAGNET

SINGLE ELECTRON TRANSISTOR

Approved by:

Dr. Dragomir Davidovic, Advisor
School of Physics
Georgia Institute of Technology

Dr. Walter De Heer
School of Physics
Georgia Institute of Technology

Dr. Carlos Sa De Melo
School of Physics
Georgia Institute of Technology

Dr. Ian Ferguson
School of Electrical and Computer Engineering
Georgia Institute of Technology

Dr. Phillip First
School of Physics
Georgia Institute of Technology

Date Approved: January 28, 2005

This work is dedicated to my mother and grandmother.

ACKNOWLEDGMENTS

I want to thank the members of the group who participated actively in this work Rupa Bhaumik and Michael Bowman and the current and former members of the group Andrei Korotkov, Changshi Lao, Cuiyun Wang, Yaguang Wei, Liyuan Zhang, Xiya Liu and Wonsang Koh.

I want to give a special thank to Ramiro Moro and Helmut Biritz who recommended me to come to the School of Physics.

Very valuable knowledge and recommendations were received from Saburo Takahashi, Andrew Zangwill, Uzi Landman, Carlos Sa De Melo, Joe Nabity, Phillip First, Kevin Brennan, John Cressler and Walt De Heer.

Support from Walt De Heer's group came from Claire Berger, Zhimin Song and Yan Yi who helped me in the utilization of the AFM. A great support was provided by Humberto Vargas in the tuning of the SEM.

I also received assistance and cooperation from Nancy Bagget, Patricia Dixon, Velera Pate, Kevin Carter, Mark Miller and Keith Garner.

TABLE OF CONTENTS

LIST OF FIGURES

LIST OF SYMBOLS

Å	Unit of length, Angstrom (10^{-10} m)
aF	atto Farad (10^{-18} F)
B	Magnetic Field
C	Capacitance
e	Electron charge (1.6 x 10^{-19} coulomb)
EBL	Electron Beam Lithography
eV	electron volt
f(E)	Fermi Distribution
FSF	Ferromagnetic/Superconducting/Ferromagnetic
G	Differential conductance
h	Planck Constant (6.62 x 10^{-34} Js)
I	Current
IPA	Isopropanol
K	Kelvin
k_B	Boltzman constant (8.6174 x 10^{-5} eV K^{-1})
M	Magnetization
MAA	MethAcrylic Acid
MIBK	Methyl Iso-Butyl Ketone
N(E)	Density of States
nm	Nanometer (10^{-9} m)
P	Spin Polarization
PMMA	PolyMethyl MethAcrylate
R	Resistance
RPM	Revolutions per Minute

sccm	unit of flow, standard cubic centimeter per minute
SEM	Scanning Electron Microscope
SET	Single Electron Transistor
T	Teslas
T_c	Critical Temperature
TCE	Trichloroethylene
TMR	Tunnel Magneto Resistance
Torr	Unit of pressure, equal to 133.32 Pa
U	Potential Energy
V	Bias Voltage
$\delta\mu$	Shift of the chemical potentials of the quasiparticles
Δ	Superconducting energy gap
Ω	Ohm
τ_E	Energy Relaxation Time
τ_s	Spin Relaxation Time
τ_t	Time between 2 consecutive tunneling events
μ	Chemical Potential

SUMMARY

This thesis describes a research of suppression of superconducting gap in a superconducting island of a Ferromagnetic-Superconducting-Ferromagnetic Single-Electron Transistor due to the fringing magnetic fields produced by the ferromagnetic leads. The devices are working below the critical temperature of the superconducting island. A model is proposed to explain how the fringing magnetic field produced by the leads is strong enough to suppress the superconducting gap. The peak of the fringing magnetic field produced by one lead reaches 5000 oe. It is observed an inverse tunneling magneto resistance during the suppression of the superconducting gap, obtaining a maximum absolute value 500 times greater than the TMR in the normal state.

It is concluded that the suppression of the superconducting gap is due to fringing magnetic field and not to the spin accumulation because the low efficiency of the spin injection. It is suggested a new geometry to reduce the effect of the fringing magnetic field so it can be obtained a suppression of the superconductivity due to the spin accumulation. It is described the qualitatively behavior of the IV characteristic when the suppression of the superconductivity is due to spin accumulation.

CHAPTER I

INTRODUCTION

Spintronics is a new area in great expansion because of its present and future applications (Wolf, 2001). This area of research is studying the behavior of the spin of the electron, a degree of freedom that is not quite used in the Microelectronics Industry and offers great opportunities for a new generation of devices combining standard microelectronics with spin effects. Although the term of “spintronics” is quite new, it has been used since the late 90’s, the basic effects and phenomena have been studied for many years.

The first step in understanding the effects of the spin on a spin polarized current was suggested by Mott (Mott,1936), who introduced the idea of 2 population of electrons with different spins (majority and minority) in a current to explain the dependence of the resistance in nickel on external magnetic field at low temperatures.

This idea was proved experimentally in 1970 (Meservey, 1970). In these experiments, a split of the quasiparticle states (Zeeman split) in a superconducting metal (detector) was obtained when an external magnetic field was applied. The split is due to the interaction between the external field and the magnetic moment of the quasiparticles in the aluminum strip. In 1971, Tedrow and Meservey proved experimentally that a ferromagnetic metal produces a spin polarized current (Tedrow,1971) which remains spin polarized even outside the ferromagnetic metal. They used the same technique that was used in 1970 but this time they used nickel instead of silver so the spin polarized current flew from the ferromagnetic metal (nickel) to a superconducting metal

(aluminum). An insulating barrier (aluminum oxide) was in between the 2 metals. In 1973, Tedrow and Meservey analyzed the currents of spin up and spin down quasiparticles and obtained the spin polarization (P) for some ferromagnetic metals such as Ni, Fe and Co. (Tedrow,1973).

In 1975, Julliere replaced the superconducting metal used in Tedrow's experiments for another ferromagnetic metal getting a ferromagnet/insulator/ferromagnet setup and measured the conductance in the parallel and antiparallel alignment between these 2 ferromagnetic leads (Julliere, 1975). He introduced the concept of tunneling magneto resistance (TMR) to express the change of the electrical resistance that exists when the ferromagnetic leads are in parallel and antiparallel alignments. TMR indicates that the tunneling current is proportional to the product of the density of states in both ferromagnetic leads.

In 1976, Aronov explained theoretically the effects of the spin polarized current in superconducting (Aronov, 1976a) and normal (Aronov, 1976b) metals. He predicted that a spin polarized current from the ferromagnetic metal would produce a nonequilibrium magnetization in the normal or superconducting metal so there would be a shift in the chemical potentials of the spin up and spin down electrons. This effect is known as spin accumulation.

The spin accumulation in a paramagnetic metal due to a spin polarized current was shown experimentally for the first time in 1985 (Johnson, 1985). Johnson measured the electric voltage induced by the spin accumulation in the detector (Aluminum). An aluminum film was used as a detector at temperatures ranging above the critical

temperature (T_c). The spin accumulation in a superconductor was detected in 1994 (Johnson, 1994) using a Nb film as a detector at temperatures ranging below T_c .

In 1988, Giant Magneto Resistance (GMR) was discovered (Baibich, 1988) and it marks the beginning of the new electronics industry based on spin. GMR has attracted considerable attention for fundamental physics as well as device applications such as magnetic recording heads and nonvolatile memory. The word “Giant” was used because the change in the electrical resistance in the material was about 100 %. The material was a compound of alternating layers of ferromagnetic and non magnetic metals (Fe and Cr) deposited using molecular beam epitaxy. After this discovery, a race for finding new magnetic materials started.

In 1994, it was discovered that Lanthanum manganite films showed a magneto resistance value as high as 10^5 % near 77 K and 1300 % near room temperature (Lin, 1994). This strong magneto resistance is called Colossal Magneto Resistance.

Using this kind of ferromagnetic compounds in a heterostructure with a superconductor and insulator as tunneling barrier, it was observed that the critical current of the superconductor film was strongly suppressed by the spin polarized current produced by the ferromagnetic film (Vas’ko, 1997 and Dong, 1997). The theory about this effect was introduced in 1999 and indicates (Takahashi, 1999) that superconductivity can be suppressed due to the spin accumulation in a Ferromagnet-Superconductor-Ferromagnet (FSF) double tunnel junction device and the suppression of the superconducting gap can be controlled by the bias voltage. This theory predicted a new magneto resistive effect consisting in an inverse tunneling magneto resistance in a

certain bias voltage range. These studies were extended to an asymmetric double tunnel junction in 2000 (Takahashi, 2000)

Later experiments have reported direct observation of the superconducting gap suppression using Co/Al/Co double tunnel junctions (Chen, 2002 and Johansson, 2003) due to the spin accumulation in the superconducting island. There were other experiments where the superconducting gap was suppressed but in these cases due to the fringing magnetic fields of the ferromagnetic lead. In these experiments it was shown that the fringing magnetic field produced by a ferromagnetic lead is strong enough to suppress the superconductivity in an underlying superconducting film. (Clinton, 1997).

In our experiments, we studied the suppression of the superconducting gap in a FSF single-electron-transistor due to fringing magnetic field that is produced by the ferromagnetic leads source and drain. The source and drain are made of Co and the island is made of Al. The experiment is performed at cryogenic temperature. The suppression of superconducting gap in the island is attributed to the fringing magnetic field produced by the ferromagnetic leads. This fringing magnetic field that has a large out of plane component during the antiparallel alignment of the source and drain leads is strong enough to suppress the superconducting gap. The results provide a method of controlling superconductivity and tunneling magnetoresistance due to the fringing magnetic field produced by the ferromagnetic leads. During the suppression we observed an inverse magnetoresistance for a specific range of bias voltage that is due to a decrease of the superconducting gap.

Chapter II points out a theoretical background that is important in the development of the experiment. In this chapter we will explain both methods of superconducting gap

suppression (due to spin accumulation and due to fringing magnetic fields). Chapter III describes sample fabrication, pre-cooling test, refrigeration and measurement techniques. Chapter IV shows our experimental results. In chapter V, a brief discussion and future projects are concluded.

CHAPTER II

THEORETICAL BACKGROUND

The goal of this chapter is to introduce some basic physical concepts that are necessary to understand the spin polarized transport in single electron transistors (SET) and how the superconductivity in the island can be destroyed due to 2 different effects: the spin imbalance and the fringing magnetic field produced by the ferromagnetic leads of the SET. To accomplish this goal, the tunneling effect in Metal-Insulator-Superconductor structures will be explained in the Section 2.1. This effect is the basis phenomenon in our SET. In Section 2.2, I will explain the concept of Single Electron Transistor and how the current flows from one lead to the other lead. The leads are called Source and Drain. In Section 2.3, we will introduce an additional characteristic of our tunneling current that is the spin transport. Because our leads are ferromagnetic metals, the current is spin polarized. In Section 2.4, we will deduce the conditions to destroy the superconductivity in the island due to the spin imbalance. In Section 2.5, we will explain the suppression of the superconductivity due to the fringing magnetic fields in a Ferromagnetic-Superconducting single junction.

2.1 Tunneling in Metal-Insulator-Superconductor Structures.

Quantum tunneling effect is predicted by quantum mechanics and its theory explains the effect when a trapped particle behind a barrier without the energy to overcome has a chance to overcoming it so there is a probability that the electrons tunnel the barrier.

This effect appears in tunneling barriers that can be insulators or vacuum barriers.

Figure 1 shows a tunnel barrier in between 2 metals. A bias voltage is applied between the 2 electrodes so the Fermi level of one of the electrodes rises over the other otherwise if there is no bias voltage applied between the 2 electrodes, the Fermi level are the same in both metals. The electrons in either electrode do not have enough energy to overcome the tunnel barrier. In classical mechanics, the barrier is a forbidden region for the electrons. But in quantum mechanics there is a non-zero probability for the electrons to tunnel this barrier so there is a probability that the electrons tunnel the barrier. This phenomenon is known as tunneling effect.

Figure 2 shows a tunnel barrier that is in the middle of a normal metal (left side) and a superconducting metal (right metal). A voltage V is applied between the metals so the chemical potential μ_1 of the normal metal rises eV over the chemical potential μ_2 of the superconducting metal. In this case the insulator layer is in the middle of two metal layers. The metal to the left is a normal metal and the one to the right is a superconductor. Because all the electrons within Δ of the Fermi energy have fallen into the superconducting state there are no electron states for the normal single electrons to tunnel into or out of unless the bias voltage exceeds Δ/e. At voltage Δ/e the electrons have many electron states available. Thus there is a sharp rise at $V=\Delta/e$. At voltage greater than Δ/e, the electrons experience the normal tunnel resistance of the tunnel junction.

To calculate the tunneling current, we must calculate the current due to electrons impinging on the barrier from normal metal 1 to superconductor metal 2 and then subtract the reverse current from the superconductor metal 2 to normal metal1. The result is the net current.

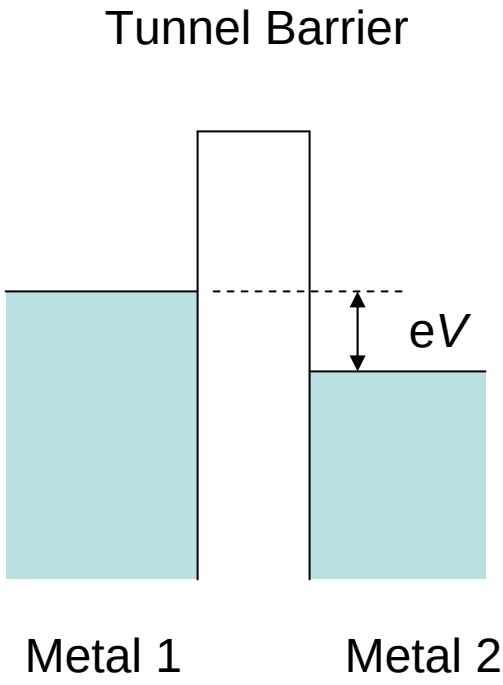

Figure 1. Tunnel junction with 2 normal metallic electrodes at T=0. Because a bias voltage is applied, the Fermi level of metal 1 is shifted over the Fermi level of metal 2. Because of quantum tunneling effects, some electrons are able to tunnel through the barrier

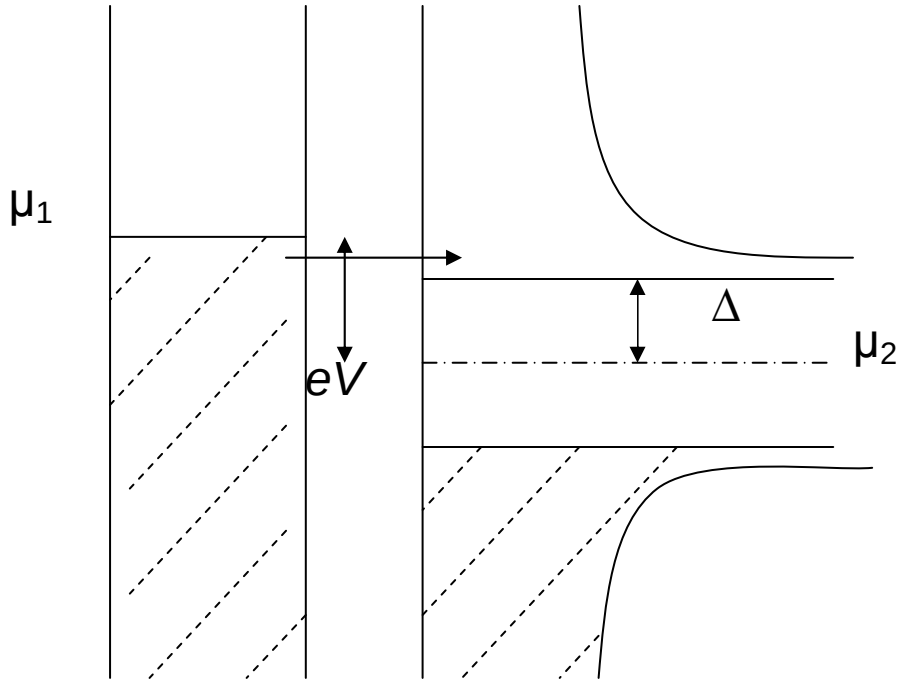

Figure 2. Density of states vs. energy. Shading denotes states occupied by electrons at T=0 and bias voltage V.

The tunneling current from metal 1 to metal 2 can be written as

$$I_{1\to 2} = A\int_{-\infty}^{\infty} |T|^2 N_1(E) f(E) N_2(E+eV)[1-f(E+eV)]dE \quad (1)$$

Where *V* is the applied voltage, *eV* is the chemical potential across the junction and *N(E)* is the appropriate normal or superconducting density of states. The factors $N_1 f$ and $N_2(1-f)$ give the number of occupied initial states and of available final states. *A* is a constant of proportionality.

The reverse current is

$$I_{2\to 1} = A\int_{-\infty}^{\infty} |T|^2 N_1(E)[1-f(E)] N_2(E+eV) f(E+eV)dE \quad (2)$$

Subtracting the reverse current from the metal 2 to normal metal 1 we get the net tunneling current

$$I = A|T|^2 \int_{-\infty}^{\infty} N_1(E) N_2(E+eV)[f(E)-f(E+eV)]dE \quad (3)$$

This is a general expression for any type of metal so this expression will be reserved for our specific case when one of the metals is a superconductor.

Considering that metal 1 is normal and the metal 2 is superconductor, we have

$$I = A|T|^2 N_1(0)\int_{-\infty}^{\infty} N_2(E+eV)[f(E)-f(E+eV)]dE$$

$$= \frac{G_{nn}}{e}\int_{-\infty}^{\infty} \frac{N_{2s}(E)}{N_2(0)} N_2(E+eV)[f(E)-f(E+eV)]dE \quad (4)$$

To solve Equation (4), numerical methods must be applied but we can infer some qualitative characteristics of the current vs bias voltage curves (IV curves). In Figure 3 we can see the qualitative behavior of the IV curve at T=0 and T>0. At T=0, there is no tunneling current until $e|V| \geq \Delta$, since the bias voltage must provide enough energy to create an excitation in the superconductor. For T>0, there is tunneling current at lower voltages, giving an exponential tail of the current in the region $e|V| = \Delta$.

2.2. Single-Electron Transistor (SET).

A single electron transistor consists of a metal island coupled to a source and a drain leads by tunnel junctions and coupled to a gate as a capacitance. The major characteristic of a SET is that the current flow in multiple number of electron charge, so we can make electrons flow one by one from source to drain while we are changing the gate voltage. The island is so small that the addition of just one electron in the island significantly changes the electrostatic energy of the island. This leads to a phenomenon called Coulomb blockade that will be explained later. The change of the electrostatic energy is known as charging energy and must be greater than the thermal energy $k_B T$.

This idea was proposed by D.V. Averin and K.K. Likharev in 1985 and is based on quantum tunneling effect.

This single electron tunneling phenomenon is observed under 2 conditions that are:

- The charging energy must be greater than the thermal energy $k_B T$ so the electrons can be fixed in the island if there is no energy applied between source and drain.

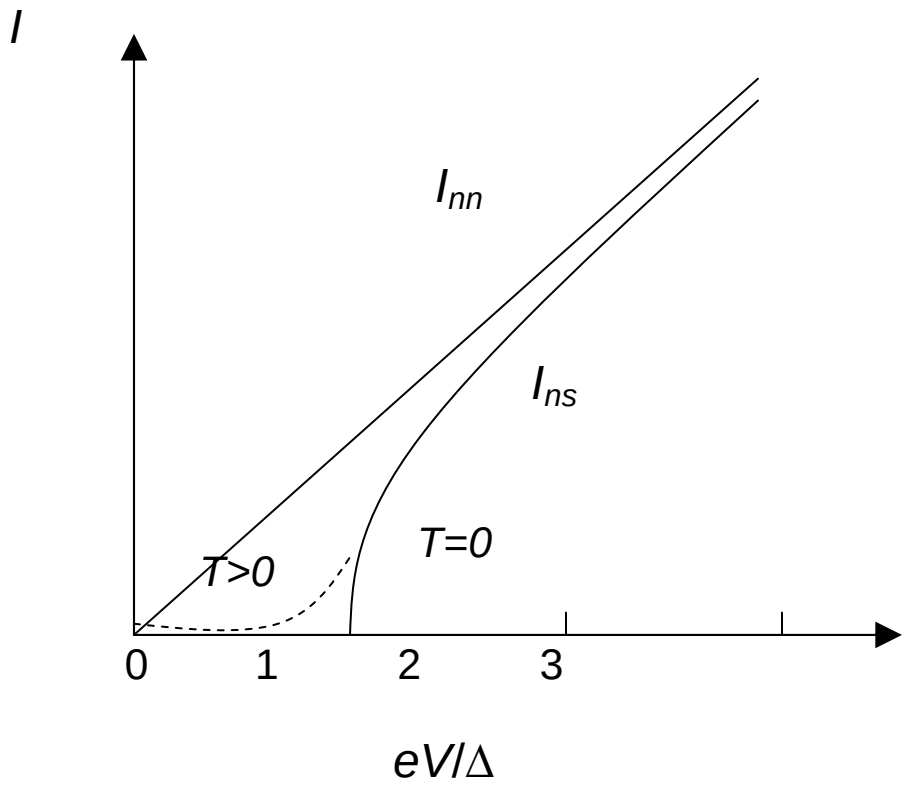

Figure 3. I-V characteristic of normal-superconductor tunnel junction. Solid line correspond to T=0 and dashed line to T>0.

- The conductance of the tunnel junction must be much less than the quantum conductance $2e^2/h$ so the electrons will not be delocalized in the island.

After Averin's idea was proposed, several groups started working in the fabrication of SET's so the first SET was fabricated in 1987 (Fulton,1987).

A preliminary work was done by Zeller and Giaever (Giaever, 1968) where the single electron charging effects in a structure were first considered in a semiquantitative way.

Figure 4 shows a schematic diagram of a SET. We can observe that the metallic island is in between the source and drain leads and separated by tunnel barriers. There are 3 significant capacitances, two of the tunneling junctions (C_1 and C_2) and one of the gate (C_g), the bias voltage applied is V_1-V_2 and the gate voltage is V_g.

2.2.1. Energy and Charging Relations.

To explain this subsection, we will use the model of an SET made of normal metals. It is under these conditions that we will get the parameters (capacitances, resistances, charging energy, etc.) of the SET.

The electrostatic potential φ of the island is

$$\varphi = \frac{\sum C_i V_i + ne}{C_\Sigma} \tag{5}$$

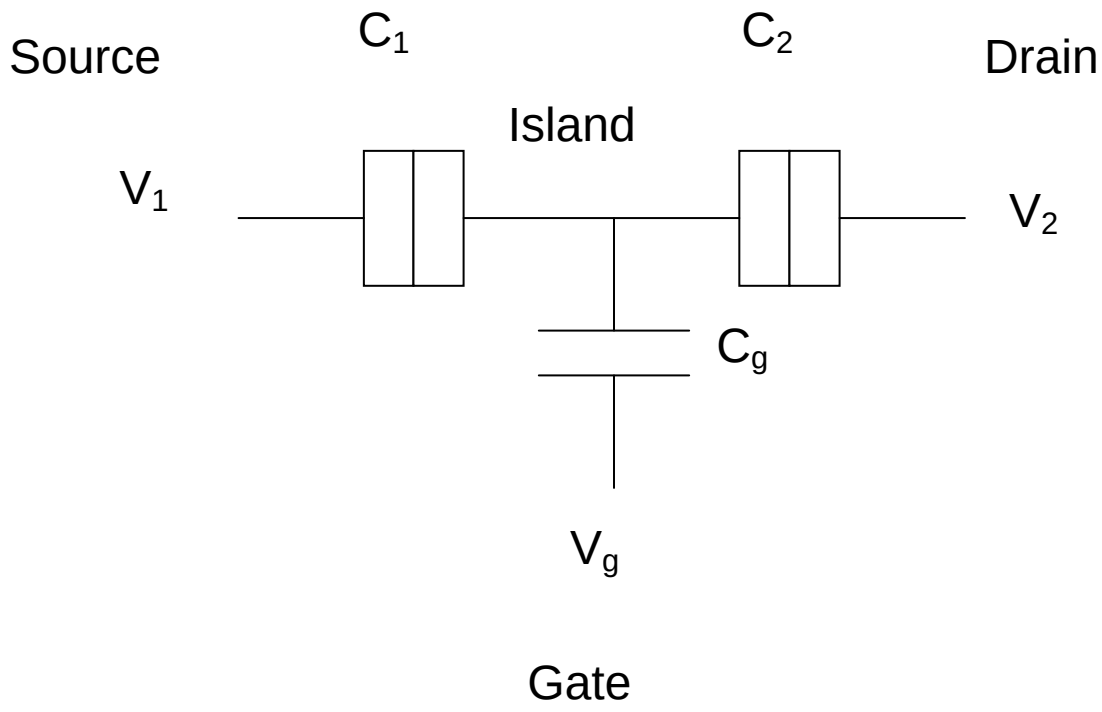

Figure 4. Schematic diagram of the single electron transistor.

where n is initial number of electrons and C_Σ is the total capacitance of the island. The total capacitance is the sum of the junction capacitances and the gate capacitance.

The electrostatic energy U is

$$U = \frac{1}{2}\sum C_i (V_i - \varphi)^2 \tag{6}$$

By using Eq. 5 for φ, we will get

$$U = \frac{1}{2C_\Sigma}\sum_i \sum_{j>i} C_i C_j (V_i - V_j)^2 + \frac{(ne)^2}{2C_\Sigma} \tag{7}$$

But to get the total energy E we have to add the work done by each voltage source. (Averin, 1991). The sum of all these contributions is

$$W_j = e\sum_i (V_j - V_i)\frac{C_i}{C_\Sigma} \tag{8}$$

Considering that n_1 is the number of electrons tunneling into the island through junction 1 and n_2 is the number of electrons tunneling out of the island through junction 2, then

$$E(n_1, n_2) = U - n_1 W_1 + n_2 W_2 \tag{9}$$

where $n=n_1-n_2$ and $Q_o=C_g V_g$

So using Equations (7) and (8) in (9) and considering a symmetric bias voltage $V_1=-V/2$ and $V_2=V/2$ we obtain that the system free energy is

$$E(n_1, n_2) = \frac{(-en + Q_o)^2}{2C_\Sigma} - [n_1 + n_2 + n\frac{(C_2 - C_1)}{C_\Sigma}]\frac{eV}{2} \tag{10}$$

where $V=V_1-V_2$

From Equation (10) we can get the energy changes $\Delta E_1^{\pm}$ and $\Delta E_2^{\pm}$ for $n \to n \pm 1$ by tunneling of an electron through junctions 1 and 2, respectively.

We get

$$\Delta E_1^{\pm} = \frac{e^2}{C_\Sigma}\{[\frac{1}{2} \pm (n - \frac{Q_o}{e})] \pm \frac{C_2 V}{e}\} \tag{11}$$

$$\Delta E_2^{\pm} = \frac{e^2}{C_\Sigma}\{[\frac{1}{2} \pm (n - \frac{Q_o}{e})] \mp \frac{C_1 V}{e}\} \tag{12}$$

Equations (11) and (12) show that the tunneling of electrons is completely blocked if $\Delta E_{1,2}^{\pm}$ is positive, considering this condition we can build the phase diagram of the double tunnel junction.

Figure 5 shows the phase diagram of the double junction. The straight lines correspond to the equations $\Delta E_{1,2}^{\pm} = 0$ for various values of n. Within each rhombic-shaped region there exists a value of n, which provides the equilibrium state of the junction. In this region there is no flow of electrons because $\Delta E_{1,2}^{\pm}$ is positive. The intersection points between the straight lines in the *Q* axis are the points where the tunneling of the electrons is favorable because the energy of n electron system is equal to the energy of n+1 electron system and both configuration qualify as the lowest state energy of the system. Outside the rhombic-shaped region there is flow of electrons because $\Delta E_{1,2}^{\pm}$ is negative.

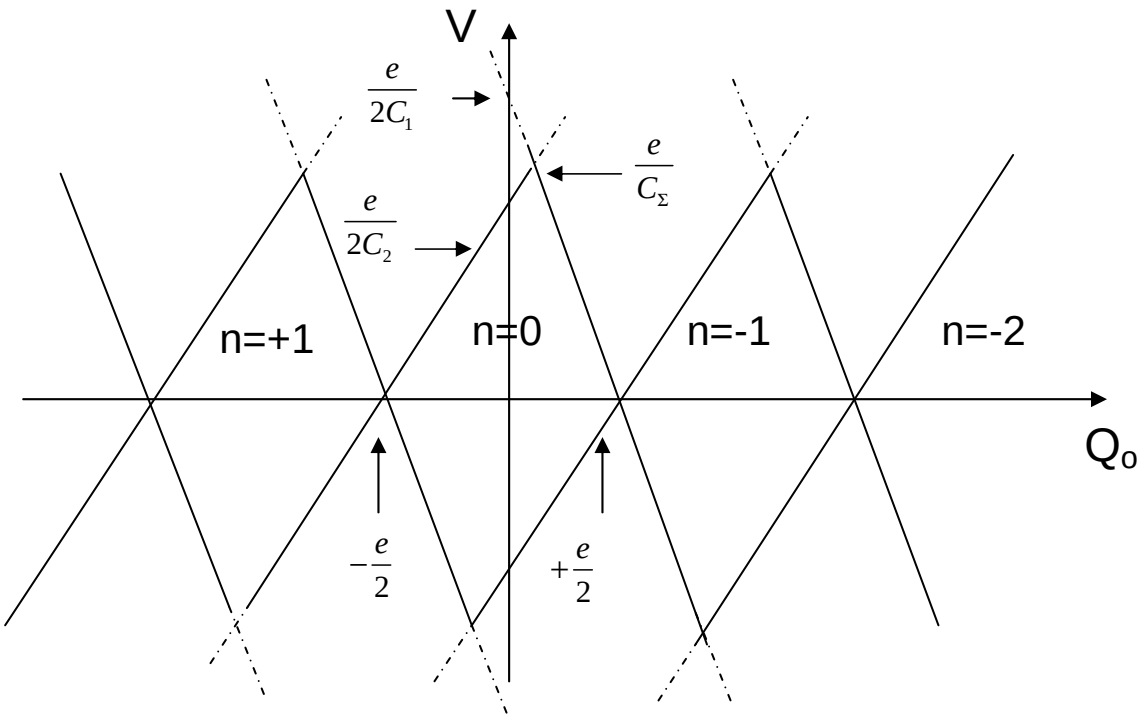

Figure 5. Phase diagram of the single electron transistor. The central rhombuses correspond to the coulomb blockade of tunneling for various equilibrium values of n.

2.2.2. Tunneling current in a SET.

As it is discussed in Section 2.2, the current passes in quantized units of the electron charge in a SET. An electron hops into the island when its energy is equal to or higher than the Coulomb energy.

At sufficiently low bias voltage, the electrons do not have enough energy to jump into or out of the island so there is no current. This effect is called Coulomb blockade and for an electron to jump into or out of the island, its energy must be equal to the coulomb energy $\frac{e^2}{2C_\Sigma}$. Figure 6a shows this case.

If we increase the bias voltage and overcome the Coulomb energy, the electrons will have enough energy to jump into the island through junction 1. The critical bias voltage needed to transfer an electron into the island is known as coulomb blockade voltage and is equal to $\frac{e}{2C_{1,2}}$ (minimum value of both) so *V* must be greater than $\frac{e}{2C_{1,2}}$ so that the electron jumps into the island. Figure 6b shows this case. Because we are adding an extra electron in the island, the Coulomb energy increases in amounts equal to the charging energy E_C.

If we keep the bias voltage below the Coulomb gap voltage and start increasing the gate voltage, the energy of the initial system increases and the energy of the system with one extra electron decreases. When the gate voltage reaches the point of maximum slope in the Coulomb staircase, both configurations equally qualify as the lowest energy states of the system. So the Coulomb blockade is broken and the electrons are allowed to tunnel

through the junctions so the electrons can jump into or out of the island. The Coulomb blockade is broken when the gate capacitance is charged with $\frac{e}{2}$ (Devoret, 1992). Figure 6c shows this case.

Figure 7 shows the IV curve of a SET. The flat region where there is no current is where Coulomb Blockade occurs because the electrons do not have enough energy to overcome the tunneling barriers. Above the Coulomb gap voltage (threshold voltage), the current starts flowing so we need to apply a bias voltage greater than $\frac{e}{2C_{1,2}}$ to make the electrons flow from source to drain. From this figure and applying the orthodox theory, we can find the parameters of the single-electron transistor.

2.3. Spin-polarized transport.

Spin polarized transport occurs in ferromagnetic metals due to the imbalance in the spin populations at the Fermi level.

The density of states in a ferromagnetic metal is shown in Figure 8a. The density of states of spin-up and spin-down electrons are almost identical but they are shifted in energy, so the net magnetic moment in the system is proportional to the difference between populations of spin-up and spin-down electrons that is why ferromagnetic metals can produce spin polarized current. In Figure 8b, we have the density of states in a normal metal. The density of states of spin-up and spin-down electrons are identical and they are not shifted in energy, so there is not net magnetic moment.

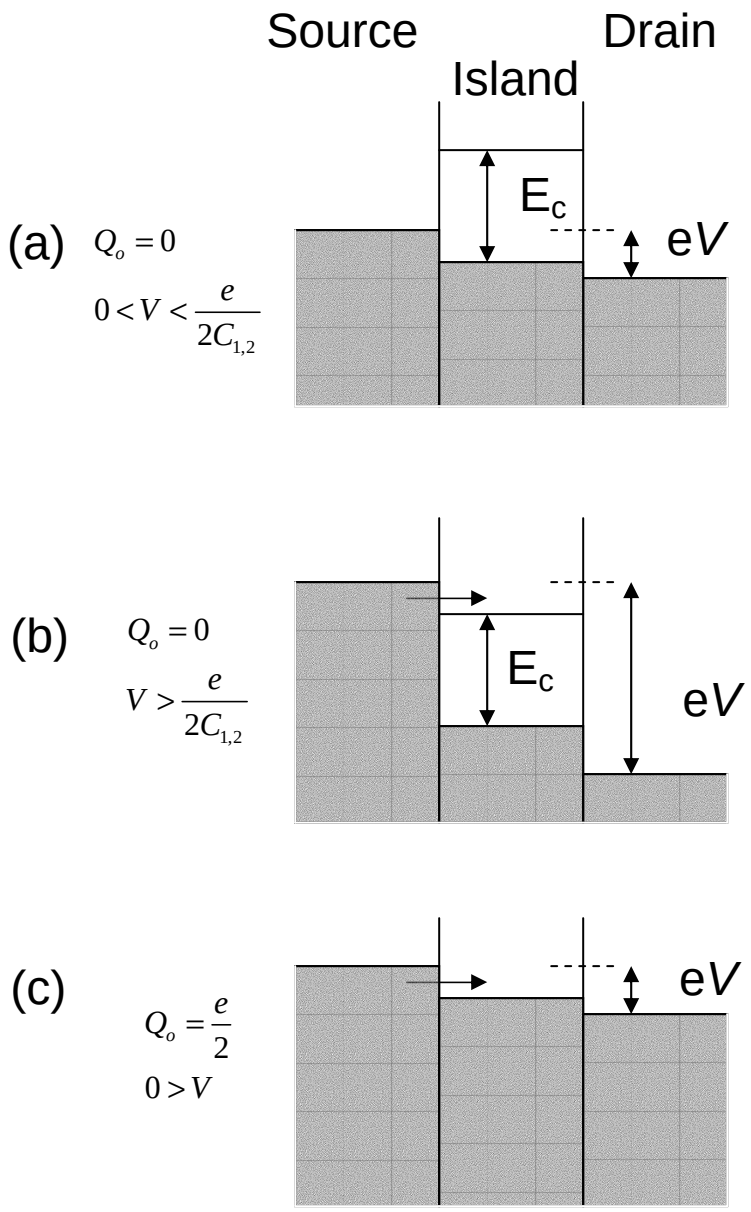

Figure 6. Energy diagrams for tunneling in a single-electron transistor. (a) Region of Coulomb blockade. (b) Tunneling when $V>e/2C_{1,2}$. (c) Tunneling when Q_0=e/2.

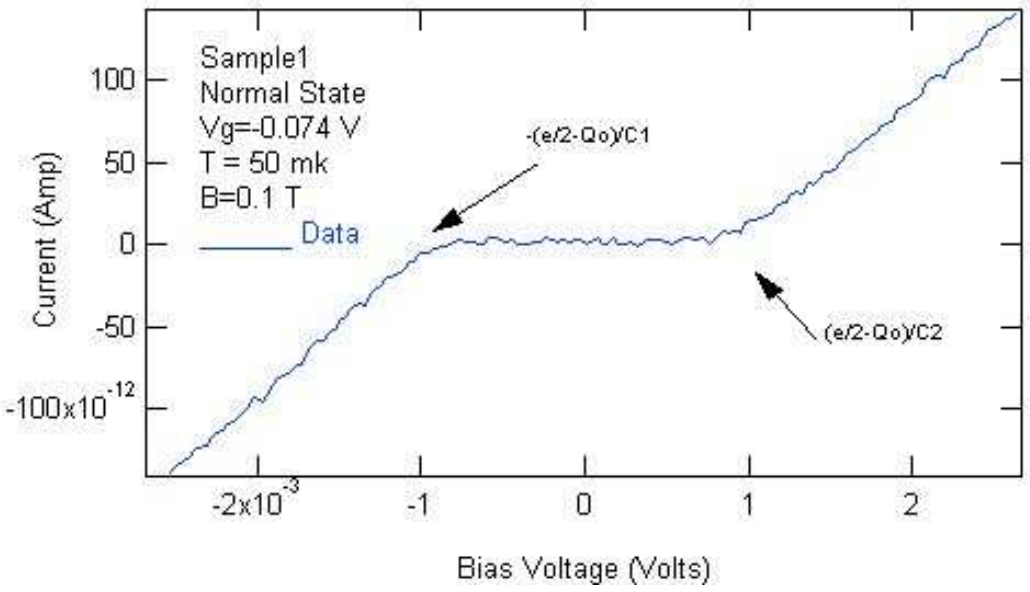

Figure 7. Current vs Bias Voltage in a Single-Electron Transistor

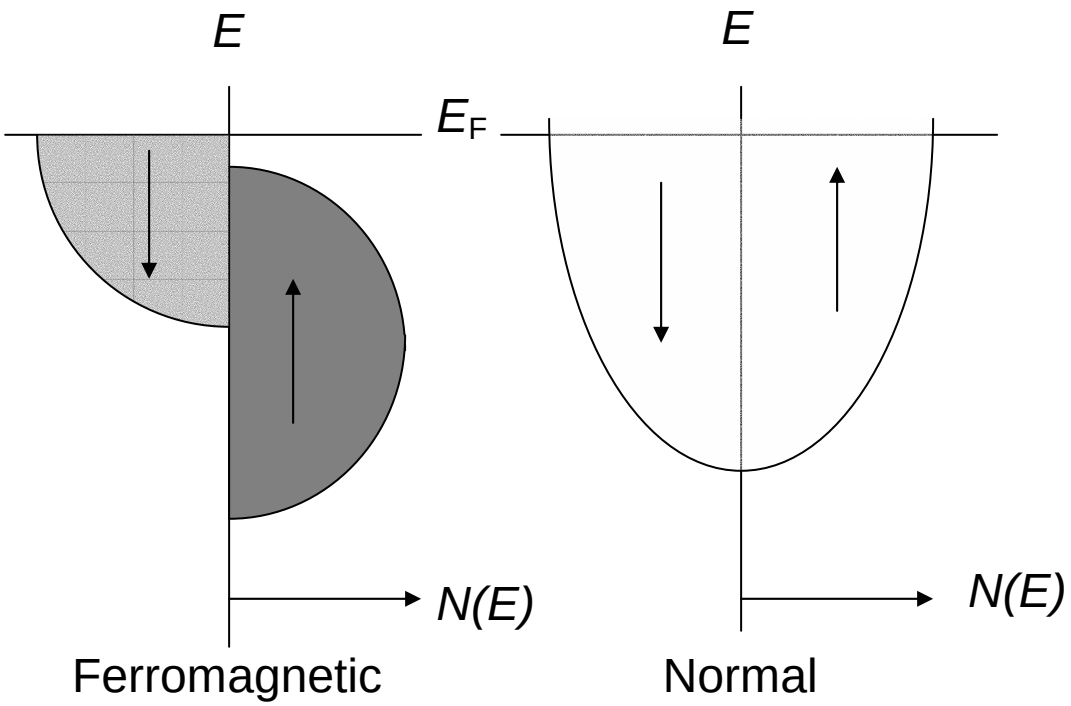

Figure 8. Density of States N(E) in a ferromagnetic and normal metals, represented schematically.

Figure 9 shows a spin-polarized SET, the source and drain are made of ferromagnetic metals and the island is made of a normal metal. The source is in the left side and the drain the right side. The electrons are jumping from source into the island and then into drain. Considering that the current is contributed by electrons with 2 spins (Mott, 1936), we can conclude that electrons with a specific spin state from the source will be accepted in the unfilled state of the same spin in the drain. We consider that there is no spin scattering or spin flip during the tunneling in the tunneling barrier that separates the ferromagnetic metals and the normal metal (Tedrow, 1971) so the electrons keep their spins during the jump from source to drain.

In the parallel state, when both magnetization moments of the ferromagnetic source and drain are aligned, the resistance is low because majority electrons will jump into unfilled majority states and the same for minority electrons. But the resistance is high when the ferromagnetic source and drain are misaligned (antiparallel state) because majority electrons from the source will not find enough minority unfilled states in the drain.

This effect is known as spinvalve effect and can be explained as the phenomenon when the resistance of the device can be changed by manipulating the magnetic moments of the leads so the magnetic moment of one lead is more difficult to reverse in an applied magnetic field than the magnetic moment of the other lead. So the easily reversed lead acts as a valve control and is sensitive to manipulation by an external magnetic field.

To express this change of the resistance when an external magnetic field is applied we will use the concept of tunneling magnetoresistance (TMR) which is defined as:

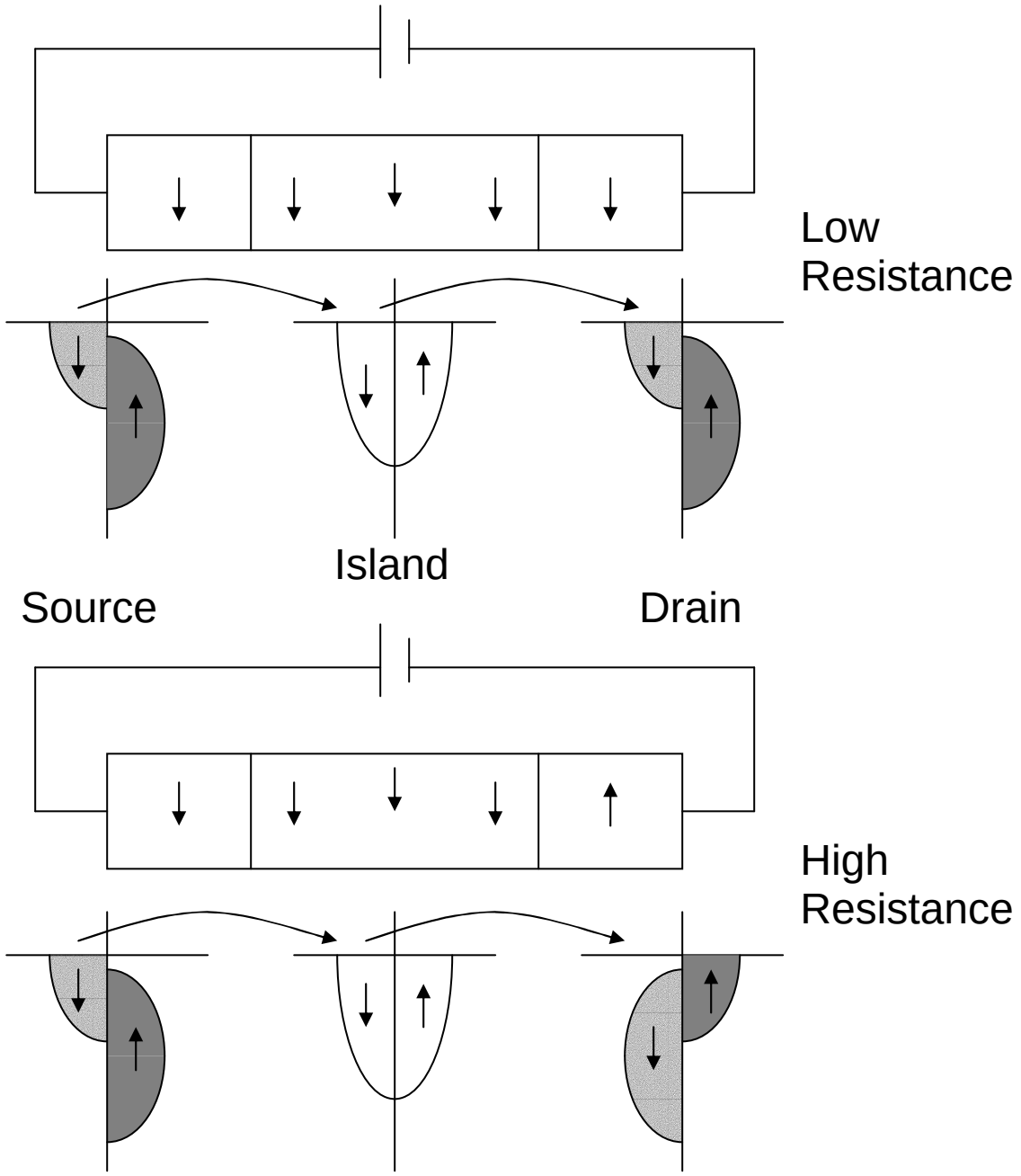

Figure 9. Schematic representation of spin polarized transport from a ferromagnetic metal to a normal metal and into a ferromagnetic metal for a parallel and anti parallel alignment of the leads.

$$TMR = \frac{\Delta R}{R_{\uparrow\uparrow}} = \frac{R_{\uparrow\downarrow} - R_{\uparrow\uparrow}}{R_{\uparrow\uparrow}} = \frac{G_{\uparrow\uparrow} - G_{\uparrow\downarrow}}{G_{\uparrow\downarrow}} \tag{13}$$

where conductance *G* and resistance *R* are labeled with the orientations of the magnetizations in the leads (Julliere, 1975).

To express the percentage of polarization of the current, the spin polarization (P) is used and is defined as:

$$P = \frac{I_{\uparrow} - I_{\downarrow}}{I_{\uparrow} + I_{\downarrow}} \tag{14}$$

where *I* is labeled with the orientations of the magnetizations in the leads.

Assuming constant tunneling matrix elements and no spin flip during the tunneling of the electrons, we can express the TMR as a function of P, yielding

$$TMR = \frac{2P_1P_2}{1 - P_1P_2} \tag{15}$$

where P_1 and P_2 are the spin polarization of the layer 1 and layer 2 respectively. (Julliere, 1975)

2.4. Spin Imbalance in Ferromagnet/Superconductor/Ferromagnet (FSF) double tunnel junctions.

According to Takahashi (Takahashi, 1999), if we have an SET with leads made of ferromagnetic metals and the island made of a superconducting metal, we will be able to suppress the superconductivity in the island due to the spin accumulation in the island while we are applying a bias voltage between source and drain.

To have the proper environment to obtain these results we have to meet 2 conditions:

- The energy relaxation time τ_E of the electrons in the superconducting island must be shorter than the time between 2 successive tunneling events τ_t so that the quasiparticles tunneling into the superconducting island will relax to the Fermi distribution and we can represent them with the Fermi function.

- The spin relaxation time τ_s is longer than τ_t so that the quasiparticles will keep their spin direction during the stay in the island and we will have a spin accumulation in the island,

If the tunnel junctions are symmetric, there will be a spin accumulation (spin imbalance) in the island (Johnson, 1985 and Johnson, 1994) in the antiparallel alignment. This spin accumulation will depend on the bias voltage applied and the spin polarization. It will provide the energy to break the Cooper pairs and destroy the superconductivity in the island.

Figure 10 shows the energy versus the densities of state of majority and minority quasiparticles for the Ferromagnet/Superconductor/Ferromagnet SET in the normal and superconducting state. The device is in the antiparallel alignment and we observe that the densities of state of the spin-up and spin-down electrons are shifted by $2\delta\mu$ (Aronov, 1976a) due to the spin accumulation in the island. This chemical potential difference $2\delta\mu$ plays the role of pair breaking energy.

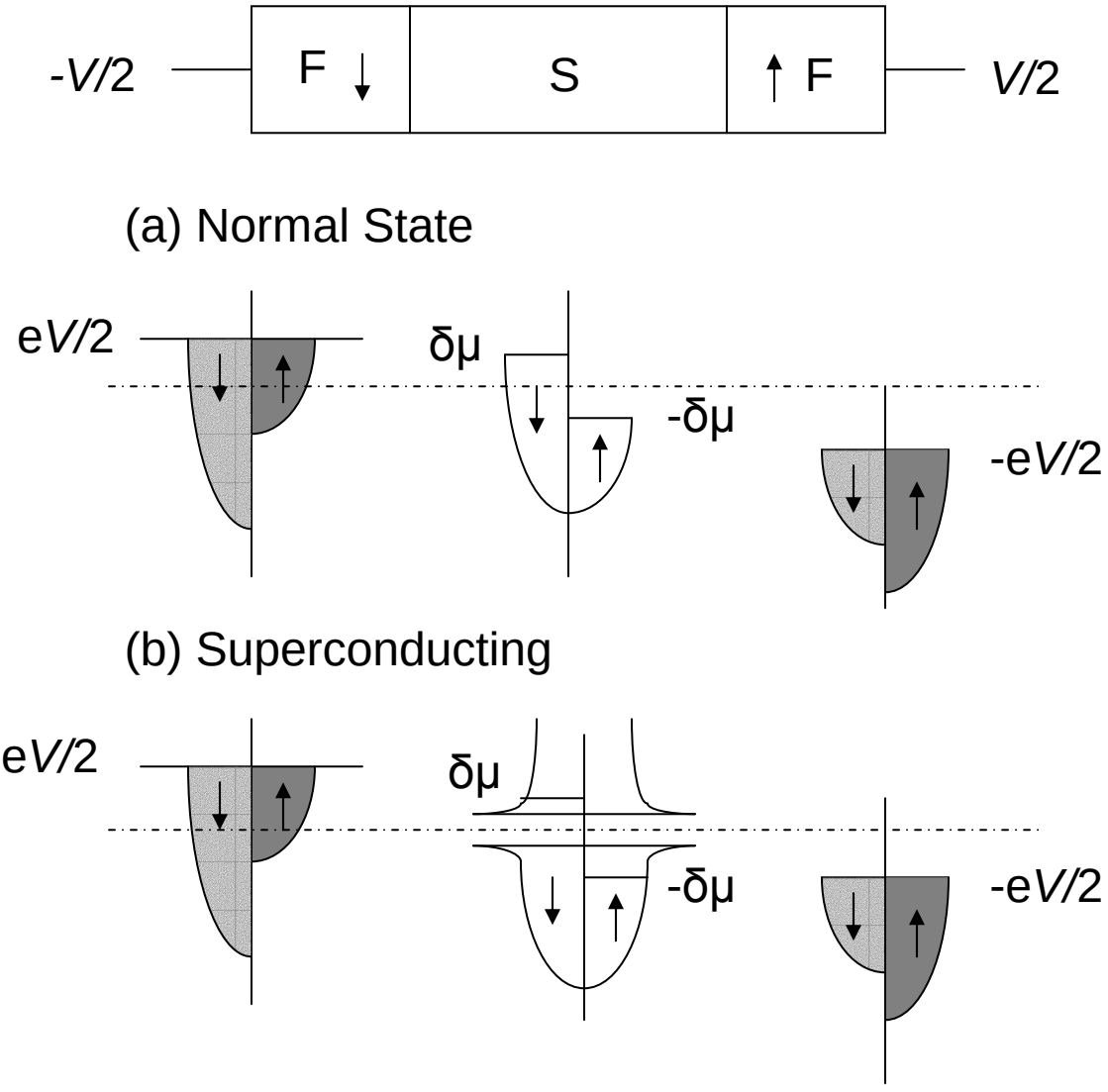

Figure 10. Schematic densities of states of a FSF device in the antiparallel alignment of the leads. (a) In the normal state and (b) superconducting state.

The distribution functions of the electrons in the superconducting island $f_{k\sigma}$, where σ is the direction of the spin are governed by the Fermi function f_o, considering that the quasiparticles relax in the island. Because of the spin accumulation (Aronov, 1976a), the chemical potentials of the spin-up and spin-down electrons are shifted oppositely by δμ from the equilibrium to produce the nonequilibrium spin density. The shift in chemical potential is due to the spin accumulation. So the distribution functions of the electrons can be written as:

$$f_{k\uparrow} = f_o(E_k - \delta\mu) \tag{15}$$

$$f_{k\downarrow} = f_o(E_k + \delta\mu) \tag{16}$$

Equation (15) represents the distribution function for spin-up electrons and Equation (16) represents the distribution function for spin-down. In the superconducting state, the superconducting gap Δ in the nonequilibrium situation can be written using the BCS gap equation (Tinkham , 1972 and Tinkham, 1996).

$$\frac{1}{D_N V_{BCS}} = \int_0^{\hbar\omega_D} \frac{1 - f_{k\uparrow} - f_{k\downarrow}}{E_k} d\xi_k \tag{17}$$

where ξ_k is the one-electron energy relative to the chemical potential.

We note that the Equations (15) and (16) are the same as that of superconductor in the paramagnetic limit (Sarma, 1963) if δμ is taken to be the Zeeman energy $\mu_B H$. Then the chemical potential 2δμ plays the role of pair breaking energy.

Besides the suppression of the superconducting gap due to the spin accumulation in the island, some other effects happen while the superconducting gap is decreasing. To explain it we can observe Figure 11. Figure 11a shows the conductance for parallel (G_F) and antiparallel (G_A) aligment vs bias voltage at T/T_c=0.4. G_F depends on the bias voltage for a constant superconducting gap. In contrast, because of the reduction of the superconducting gap in the antiparallel alignment, G_A increases faster than G_F and forms a higher peak than G_F and then decreases steeply.

Figure 11b shows the TMR vs bias voltage. The TMR is calculated using the values of G_F and G_A shown in Figure 11a. Because of the faster increase of G_A compare to G_F, there is a range where the TMR is inverse so the TMR is negative, getting a deep negative depth when $eV/2\Delta_o$~1. It is in this moment that the superconducting gap steeply decreases. When the bias voltage reaches a value which will be called as critical bias voltage (V_c) , the superconducting gap is zero and G_A jumps to the conductance G_A^N in the normal state. Because of this jump, the TMR is enhanced dramatically showing a peak.

These effects are expected to be observed when the superconducting gap is suppressed due to the spin accumulation:

- An enhancement in the TMR when the superconductivity is broken

- An inverse magnetoresistance in some range of bias voltage when the superconducting gap starts decreasing.

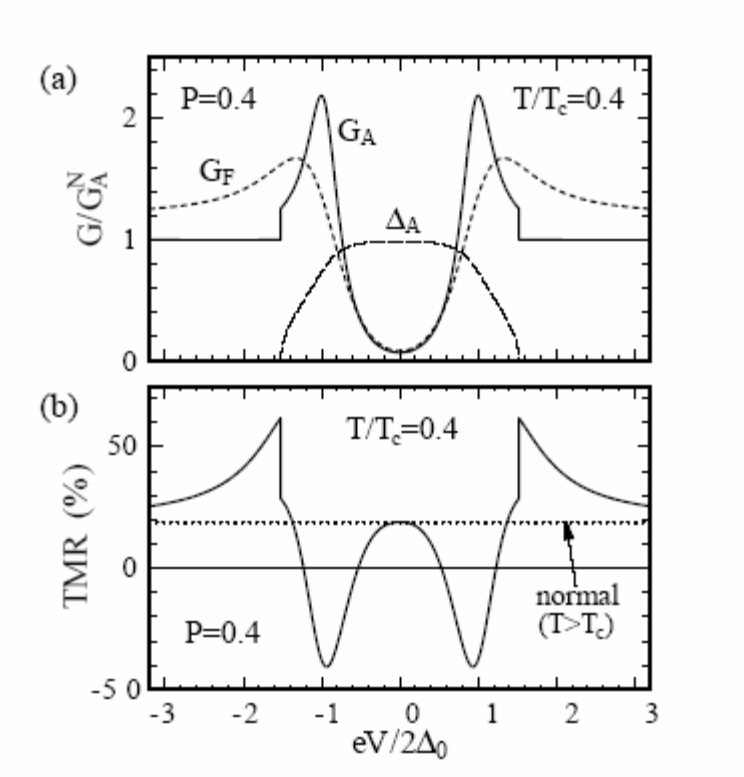

1

Figure 11. (Takahashi, 1999) (a) Tunnel conductance as a function of bias voltage for P=0.4. The solid line represents the tunneling conductance in the antiparallel alignment (G_A) and the dashed line corresponds to the parallel alignment (G_F). (b) TMR as a function of bias voltage. The dotted line represents the TMR in the normal state.

2.5. Fringing Magnetic Field in Ferromagnet/Superconductor (FS) single tunnel junction.

Figure 12 (a) shows a Ferromagnet/Superconductor single tunnel junction. A Ferromagnet/Superconductor single tunnel junction consists in a ferromagnetic layer that is in the top and a superconducting layer that is in the bottom. Both layers are divided by a thin insulator that works as tunnel barrier. Because of the ferromagnetic layer, a fringing magnetic field is produced by the magnetization M of the ferromagnetic layer and can be characterized by magnetic poles at the edges of the ferromagnetic layer. The magnetic lines are sketched in the Figure 12 (a) as solid arrows. The field magnitude is large at positions near the poles (edge of the ferromagnetic layer) and weak at remote positions.

The perpendicular component B_z is given by

$$B_z = \frac{2M_s d_F z}{(x^2 + z^2)} \tag{18}$$

with z measured from the midpoint of the ferromagnetic layer (Clinton, 1999), d_F is the thickness of the ferromagnetic layer and M_s is the saturation magnetization. The component B_z has a large magnitude and a spatial profile that decays on the order of a fraction of a micron as we can see in Figure 12 (b). To get Figure 12 (b) we use the parameters used in our experiments so for cobalt, with $4\pi M_s(Co) = 16\,\text{kG}$ (Clinton, 2000), and for typical value of d_F (~200Å in our case) the peak value of B_z is about 5000 Oe at the top surface of the superconducting layer and then starts decaying when we are moving far away from the edge of the ferromagnetic layer. So a portion of the superconducting film beneath an edge of the ferromagnetic layer should be significantly affected by the relatively strong magnetic field. In the case of Al that is used as our

superconducting film, the critical magnetic field where the superconductivity is destroyed is approximately 100 Oersted (Ashcroft, 1976).

The analysis is done for a ferromagnet/superconductor single tunnel junction, in the case of a FSF SET that consists of a double ferromagnet/superconductor tunnel junction, the resulting fringing magnetic field will be the result of the superposition of the fringing magnetic field produced by each lead (source and drain) so a major portion of the superconducting film should be significantly affected by the strong fringing magnetic field produced by both leads.

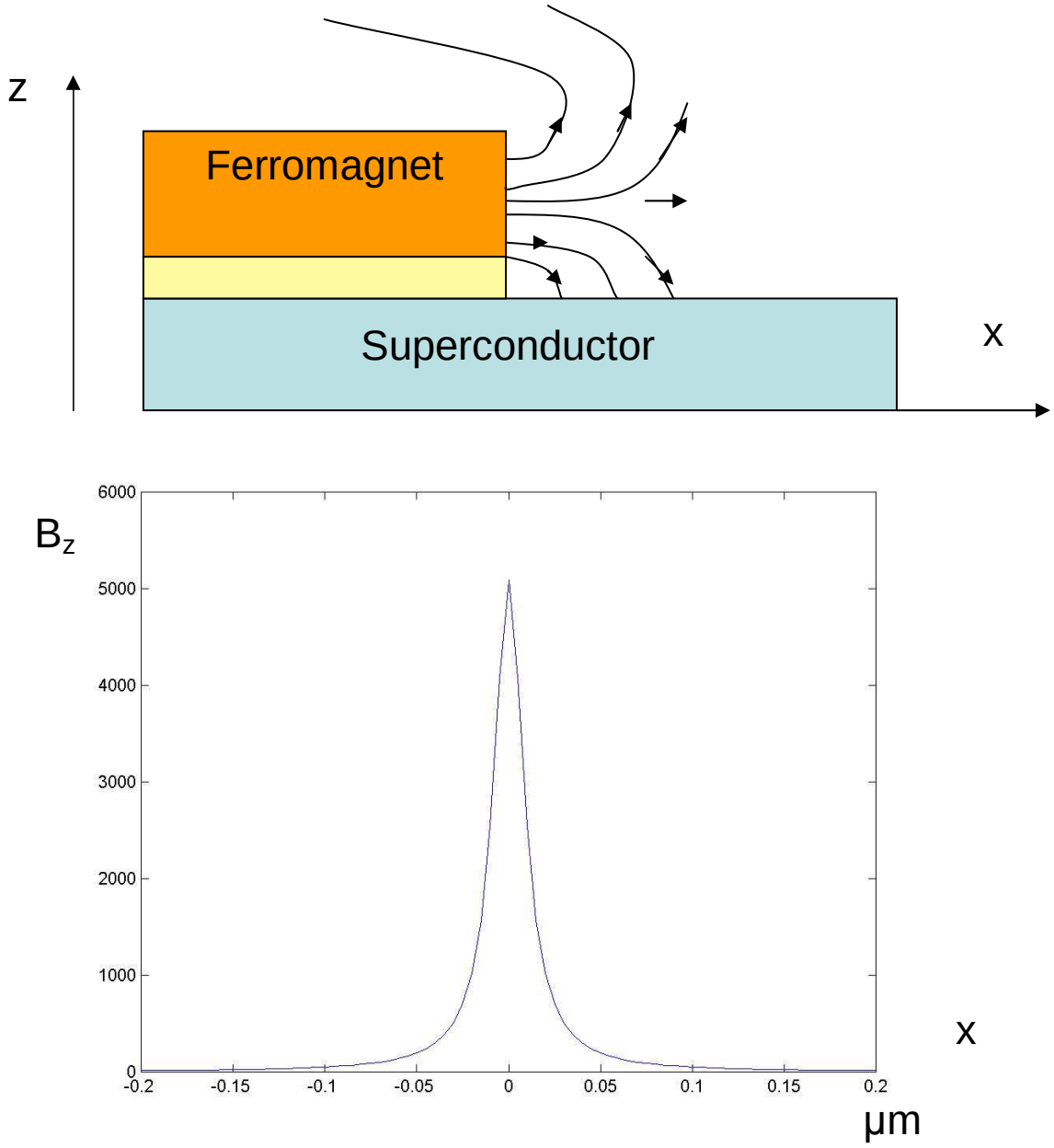

Figure 12 (a) Cross section of the ferromagnetic film showing magnetic fringe field (b) Profile of B_z beneath the edges of the ferromagnetic film.

CHAPTER III

SAMPLE FABRICATION AND MEASUREMENT PROCEDURES

3.1 Sample Fabrication.

The FSF SET's are fabricated using polished silicon wafer with a thermally grown oxide layer of approximately 1000 Å which gives a high resistance between any 2 points on the surface of the wafer. The advantage of this high resistance is that we can test our devices at room temperature without going to cryogenic temperature; the disadvantage is that we can easily blow the device because of the electrostatic discharge. One alternative to avoid electrostatic discharge is to use silicon wafer with a native oxide layer (~30Å) because the substrate shorts out our devices at room temperature protecting the devices of any electrostatic charge effect. The disadvantage of this choice is that we have to dip our devices into liquid Helium to test the functionality of them. We decided to use silicon wafer with a thermally grown oxide layer and handle and test our devices carefully following a safety procedure to avoid any damage because of electrostatic discharge effects.

3.1.1. Resist Film Preparation.

The silicon wafer is ultrasonically cleaned in trichloroethylene (TCE) followed by acetone and isopropanol (IPA) for 15 minutes in each solution. Then the wafer is blown dry using compressed dry N_2. After this cleaning procedure, the wafer is ready to be coated.

The resist is a compound of long chain polymer which is sensitive to an electron beam. There are 2 types of resist: positive and negative. When exposure of the chain polymer leads to a chain scission, the polymer dissolves in the developer. This polymer is a positive resist. If exposure of the chain polymer leads to a cross link so the exposed material is resilient to the developer and the unexposed region is etched away, it is considered to be a negative resist. We use positive resists. These resists are polymethyl methacrylate (PMMA) 950,000 molecular weight (950k) resins in 2% chlorobenzene for the top layer and a copolymer methacrylic acid (MAA) 10 % in Ethyl Lactate for the bottom layer.

We use a shadow evaporation technique (Dolan, 1977) during the fabrication of our sample so it is important to have a large undercut. To achieve a large undercut we use a bilayer resist. A bilayer resist consist in coating the wafer with 2 different resists, with a sensitive resist (MAA) as the bottom layer and a less sensitive resist as the top layer (PMMA). Because the bottom layer is more sensitive than the top layer, the exposed area in the bottom layer is larger than the affected area in the top layer. Figure 13(a) shows the cross section of our coated wafer and how the resists are affected by the e-beam. Figure 13(b) shows the cross section after being developed. We observe that more area is etched in the bottom layer obtaining the desired undercut.

The procedure of coating the wafer is as follow: First we apply the bottom layer MAA 10% in Ethyl Lactate and spin at 2000 RPM for 60 seconds. The spin speed lets us get a bottom layer of approximately 6000 Å. It is then baked at 150 ℃ for about 10 minutes in a hot plate to dry off the resist solvent. Then we apply the top layer PMMA 950K in 2% chlorobenzene and spin at 4000 RPM for 60 seconds. The spin speed lets us get a top layer of approximately 600 Å. It is then baked at 180 ℃ for about 10 minutes on a hot

plate to dry off the chlorobenzene. After being coated, the wafer is diced up by hand into small squares of dimensions 7 mm by 7 mm approximately.

3.1.2. Electron-Beam Writing and Development.

Electron Beam Lithography (EBL) is a specialized technique for creating high resolution patterns. The technique consists of scanning a beam of electrons across a surface covered with a resist film sensitive to those electrons, thus depositing energy in the desired pattern in the resist film. The feature of having an extremely small electron probe size is what lets us create high resolution patterns.

The electron-beam lithography equipment that is used is a Scanning Electron Microscope JSM 5910. This machine is controlled by Nanometer Pattern Generation System (NPGS) software during the writing of the patterns. It is this software (NPGS) where we set all our parameters to write properly on our samples.

The writing parameters include beam current, center to center spacing, line spacing, dosage and magnification. We use DesignCAD LT 2000 to design our devices.

We divide our design in 4 layers from small features (order of nanometers) to contact pads (order of millimeters). The first and fourth layers are shown in Figure 14. In Figure 14(a), we observe that area of our device, including contact pads, is approximately 1.3 mm^2. Figure 14(b) shows the finest feature of our device. The source and drain are designed to have different dimensions so that their magnetic moments are different (switch of magnetization at different external magnetic field). The gap between source and drain is about 100 nm.

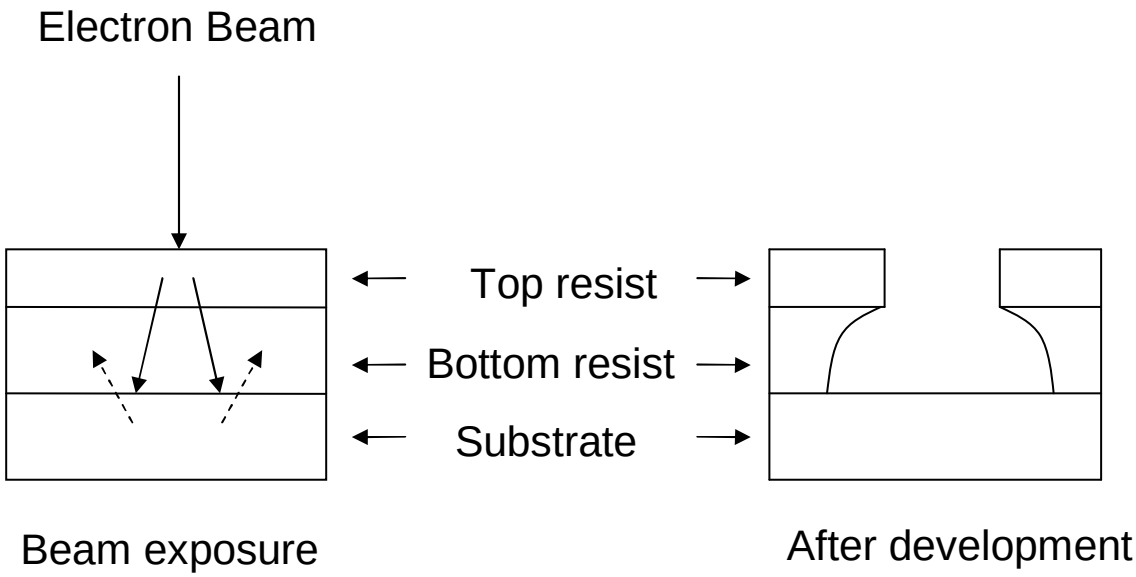

Figure 13. (a) Exposure of the resists (b) Resist profile after development.

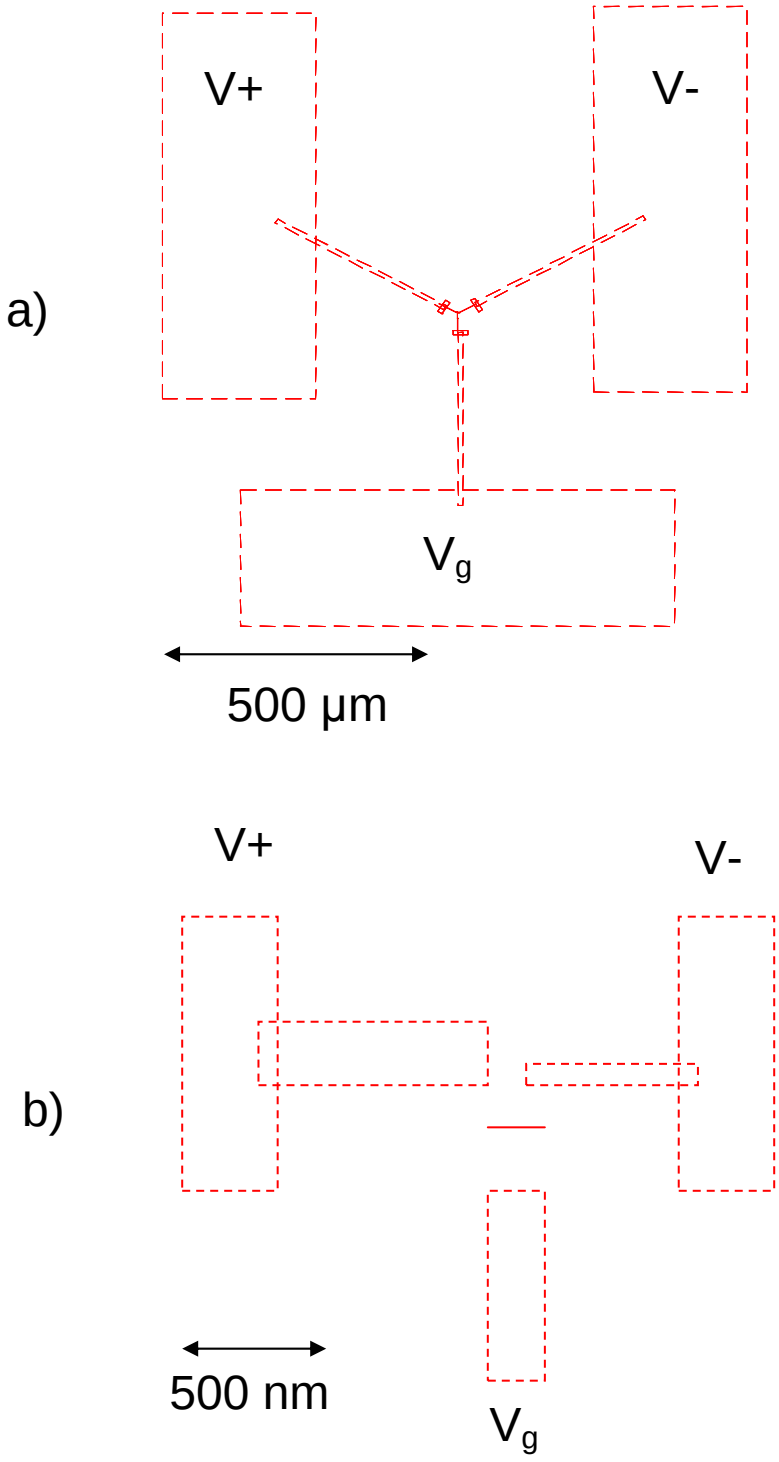

Figure 14. Design of our device (a) Large-scale view of the whole device (b)Small-scale view of the finest feature.

We use different set of parameters for each layer in the e-beam writing.

For the first layer, we use a probe current of 10 pA, a line dose of 1.8 nC/cm, an area dose of 380 μC/cm^2, a center-to-center distance of 15.91 Å, a line-to-line distance of 31.82 Å and a magnification of 1000x. For the second layer, we use a probe current of 20 pA, an area dose of 400 μC/cm^2, a center-to-center distance of 20.25 Å, a line-to-line distance of 40.50 Å and a magnification of 1000x. For the third layer, we use a probe current of 1 nA, an area dose of 400 μC/cm^2, a center-to-center distance of 130.19 Å, a line-to-line distance of 130.19 Å and a magnification of 100x. For the fourth and last layer, we use a probe current of 8 nA, an area dose of 400 μC/cm^2, a center-to-center distance and a line-to-line distance of 289.31 Å and a magnification of 65x. We work at a working distance of 15 mm.

After writing our sample, we proceed to develop it in a solution of Methyl Iso-Butyl Ketone (MIBK) and IPA, the ratio is 1:3. The sample is developed for 65 seconds and then it is rinsed with IPA for 20 seconds.

Figure 15 sketches the top view of our sample after development. The dark area is a completely uncovered area where there is no resist on top so the silicon surface can be affected directly during the evaporation. The white area is what it is called undercut and consists of the suspended top resist. The bottom layer has been removed during the development process so it is formed only by the top layer. We have an undercut below it so we can use this area for the shadow evaporation. The dashed area is an area that is not affected by the electron beam so after development, it is still covered by the bilayer resist.

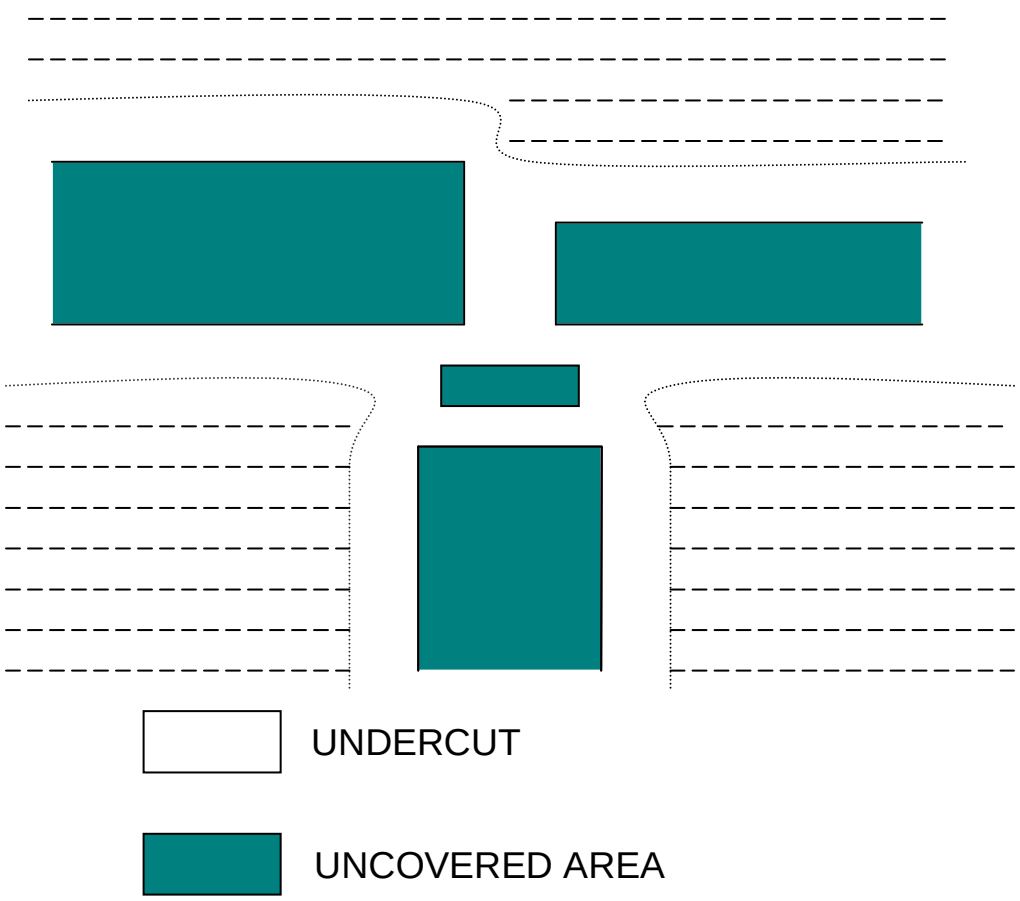

Figure 15. Top view of our sample showing the smallest feature (order of 400 nm). The white area has only the top layer (PMMA), below it there exists an undercut. The dark area is completely uncovered and the dashed area has both resist layers.

3.1.3. Metal Evaporation Procedure.

We load our sample in a rotary stage to do shadow-evaporation. The desired angles of evaporation are controlled by 2 screws that act as stoppers. A speedometer cable is connected to the stage so we can change the angles.

We deposit the different metals using a thermal evaporator. The metals to be deposited are aluminum (Al), cobalt (Co) and copper (Cu) and are loaded into containers called boats which are heated later by an applied voltage. We use 2 different types of boats: one for Copper that is made of tungsten and another for Cobalt and Aluminum that is made of tungsten too but it is coated with alumina. Alumina coating avoids these materials (Co and Al) to react with the tungsten.

The evaporator is pumped until the pressure reaches 3 x 10^{-7} Torr. To reach this pressure we leave the evaporator pumping overnight with the samples inside it. We deposit 200 Å of aluminum at 4.1 Å/sec to make the superconducting island. The angle of evaporation is +15°. To make the tunneling junctions, the aluminum is oxidized at 100 mtorr introducing oxygen (O_2) with a flow rate of 200 sccm (standard cubic centimeters per minute). The 100 mtorr is kept for 5 minutes and then the evaporator is pumped until it reaches 3 x 10^{-7} Torr again. A second evaporation is done at -15° angle to build the magnetic source and drain. 200 Å of cobalt is evaporated at a rate of 3.2 Å/sec. At the end we deposit 100 Å of copper at the same angle. The rate of copper deposition is 4.5 Å/sec. A top view of our sample in different steps of the fabrication process is shown in figure 16. Figure 16(a) shows the first evaporation at 15° angle and the Figure 16(b) shows the second evaporation at -15° angle.

(a) 15° evaporation (Al 200 Å) followed by an oxidation at 200 mtorr for 5 minutes

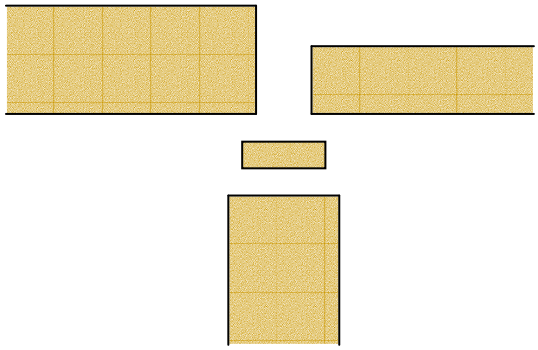

(b) -15° evaporation (Co 200 and Cu 100 Å)

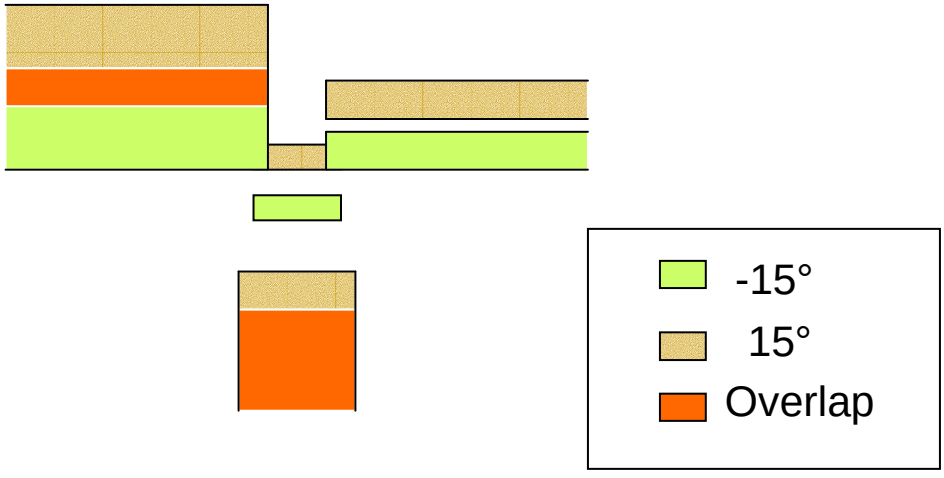

Figure 16. (a) First, 200 Å of Aluminum is deposited at 15° from the horizontal substrate, followed by an oxidation (b) Second and third evaporation at -15° of 200 Å of Cobalt and 100 Å of Copper respectively.

After evaporation, our samples are immersed in acetone for 15 minutes. The metal lines that were deposited directly on the silicon wafer remain, while the metal deposited on the resist lifts off of the wafer as the resist dissolves. Then the sample is rinsed in acetone and IPA for about 2 minutes, and then it is dried off using N_2 for 90 seconds.

A schematic 3D of our SET is shown in Figure 17 and 2 pictures at 45 kx and 20 kx are shown in Figure 18. In Figure 18 (a), we can observe in detail our SET which has 2 ferromagnetic source and drain leads, the dimensions are different so the switching magnetic fields are different and we can get a antiparallel state while we are sweeping the magnetic field. The source is a rectangle with a length of 2.5 μm and width of 500 nm and the drain is a rectangle with a length of 1.2 μm and width of 300 nm. The island has a length of 180 nm and width of 80 nm. The separation between drain and source is approximately 100 nm. We can observe the shadows that are created due to the 2 angle evaporation. The dimensions of the source and drain leads are different because we want the switching magnetic field of the magnetic moments of the leads to be different so we obtain an antiparallel alignment in a specific range of external magnetic field.

3.2. Sample Testing at room temperature.

We are able to test our samples at room temperature because a silicon wafer with a thermally grown oxide on the top is used. The bias and gate voltage are supplied through a voltage divider box. The output voltage is set using a toggle switch to select the proper resistor for the voltage divider and in that way a voltage of order of mV is applied. We use a DC voltage source. The bias voltage is 10 mV and is applied through source and drain, source and gate and drain and gate.

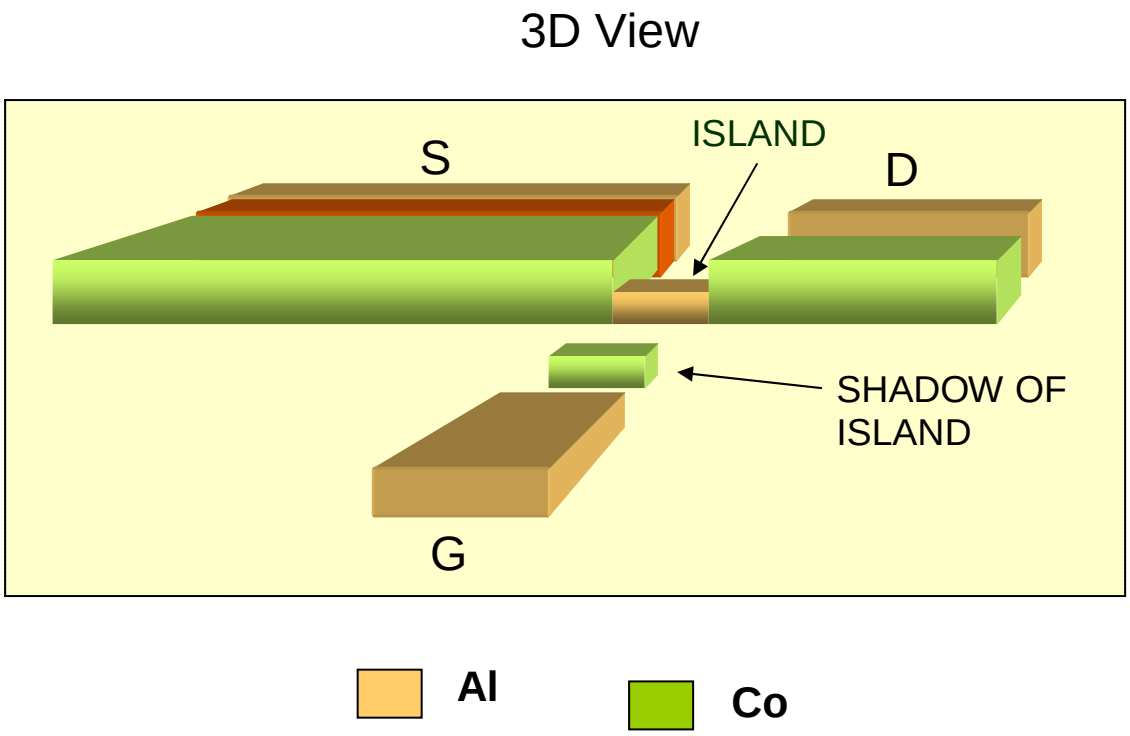

Figure 17. Schematic 3D diagram of our SET.

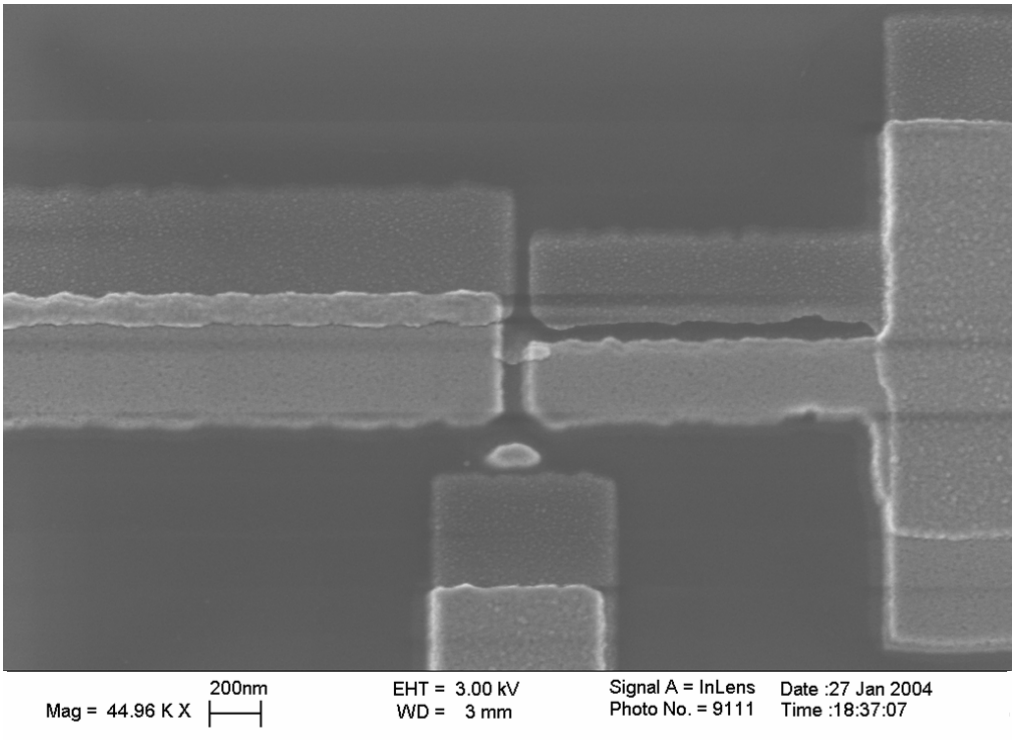

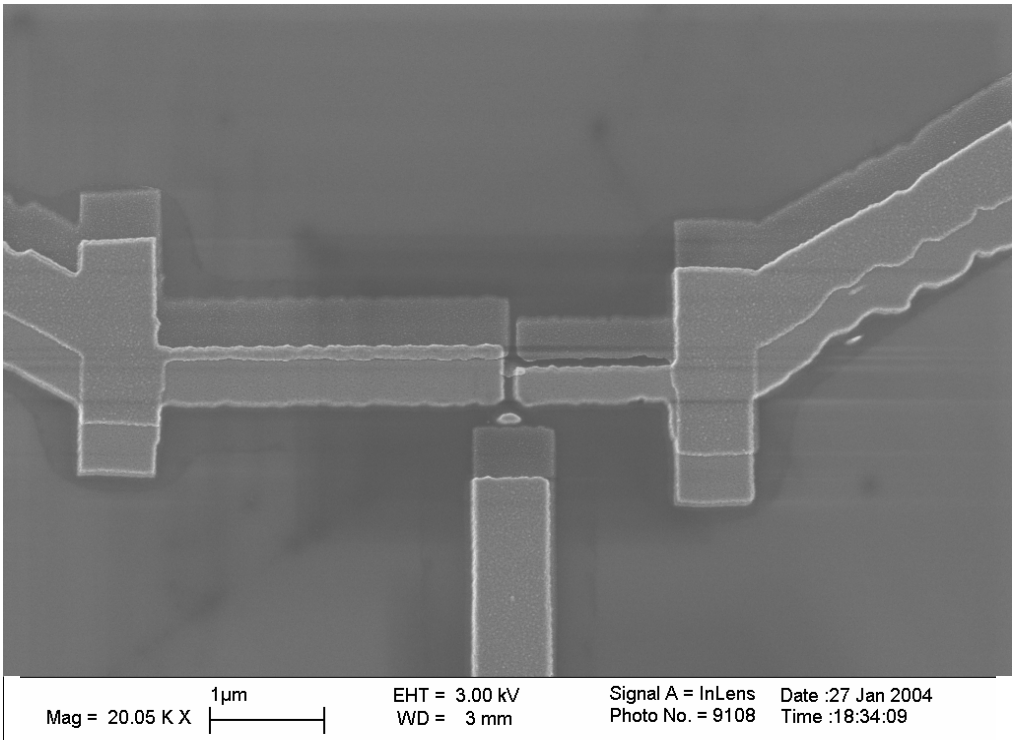

Figure 18. Pictures of our device using a scanning electron microscope (a)With a magnification of 45kx and (b) with a magnification of 20 kx.

We use a 2 probe circuit measurement to measure resistance between each pair of electrodes (source and drain, gate and drain, and gate and source). The schematic of the circuit is shown in Figure 19. We can observe that 2 voltage dividers are used to apply voltage between source and drain and between the gate and source. The applied bias voltage is set to 10 mV to avoid blowing our samples. The current is measured by a low noise Ithaco 1211 current amplifier that is set in serial with the circuit. We use a micro manipulator to make contact in the contact pads of our samples. The resistance between source and drain is in the range from 500 kΩ to 4 MΩ. The resistance between source and gate and the resistance between drain and source are always greater than TΩ range (open circuit).

3.3. Sample Mounting.

After testing our samples, we proceed to mount them on a sample holder which is designed to facilitate the electrical connection from the top of the fridge to the bottom of the "insert".

A schematic of a sample holder is shown in Figure 20. The sample holder is made of a printed circuit board which was etched in ferric acid for about 15 minutes. The dimensions of the sample holder are approximately 9mm wide and 15 mm long. A 4-pin Microtech female connector is soldered to the small piece of board. The pins are distributed as follows: 1 pin for V+, 1 pin for V- and 1 pin for V_g. The fourth pin is a spare pin.

The samples are placed on the sample holders with a layer of Apiezon N vacuum grease applied to their backs.

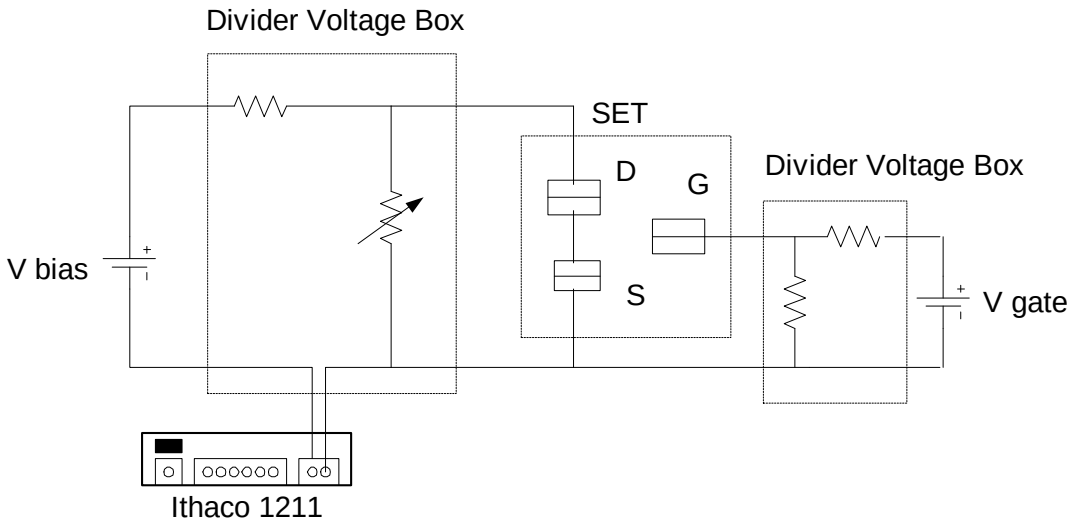

Figure 19. Schematic of electrical measurement circuit at room temperature.

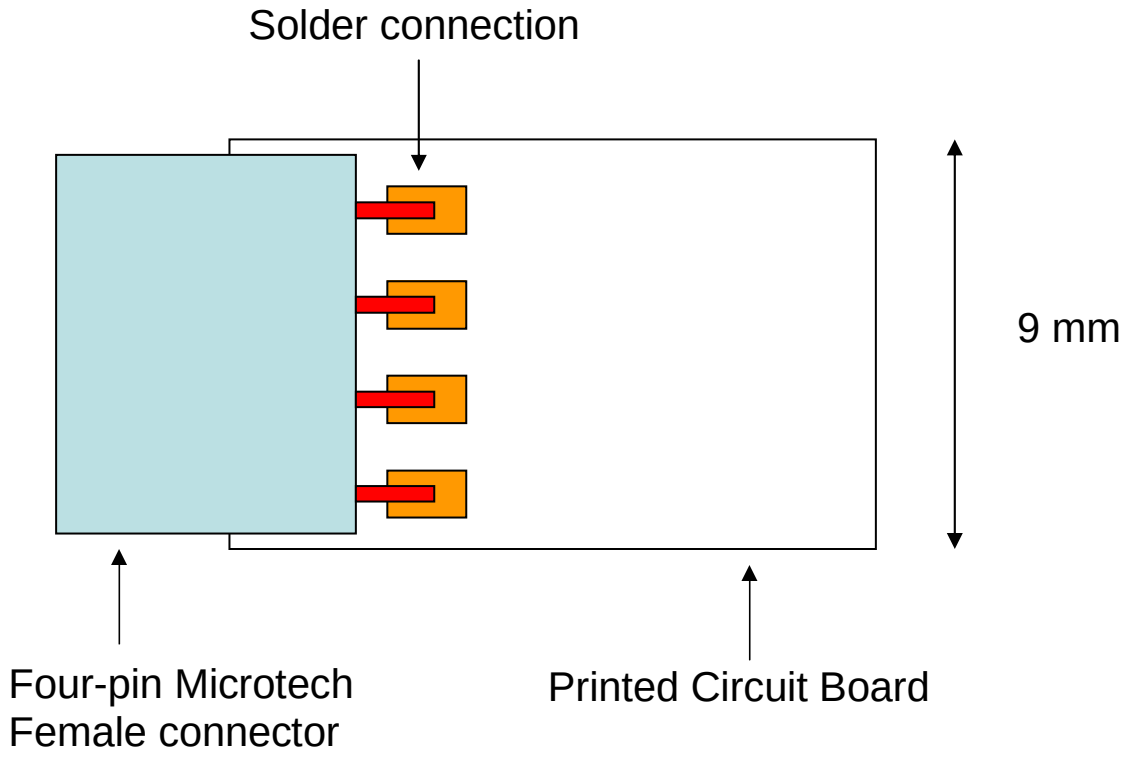

Figure 20. Top view of the sample holder where our samples are mounted.

To connect the contact pads of our sample to the point contact in our sample holder, we use thin non-insulated wires. To connect this wire with the contact pads, we use indium dots pressed with a small allen tool. Because indium is very malleable, it is easy to press against the contact pad. After pressing the indium dot sticks to the contact and the wire is in between. All the tools that are used to make these connections are grounded to avoid blowing our samples.

3.4. Cooling down the samples.

After mounting the samples in the sample holders, we load the samples in the dilution fridge to cool down. The dilution fridge is the equipment which let us work at cryogenic temperatures. The principle of operation is as follow, when a mixture of 2 stable isotopes of helium (^{3}He and ^{4}He) is cooled below a critical temperature it separates into 2 phases. The concentrated phase is lighter and rich in ^{3}He and the dilute phase is heavier and rich in ^{4}He. Since the enthalpy of the ^{3}He in the 2 phases is different, it is possible to cool by evaporating the ^{3}He from the concentrated phase into the dilute phase. The principle of operation was proposed by London (1951).

The dilution fridge is in an electromagnetically shielded room to avoid any radiation to our samples and can reach a base temperature of 15 mK. The cryostat is equipped with a 14 T superconducting magnet. In our experiments the magnetic field range applied is from -0.2T to 0.2T.

After assembling the system, we test our samples to verify that they do not blow them. The tests are the same that we perform at room temperature after liftoff. We start cooling

down the system first to 77 K filling up the main bath with liquid nitrogen and leaving overnight. The next day we pump out the liquid nitrogen with helium gas and fill up the main bath with liquid helium.

At this point our system must be at 4.2 K and we can start condensing the mixture (^{3}He and ^{4}He) and cooling down to base temperature (15 mK).

CHAPTER IV

EXPERIMENTAL RESULTS

4.1. Gate Voltage Sweep at low Bias voltage.

As it was discussed in Chapter 2, when we apply a small bias voltage (bias voltage less than coulomb gap voltage) in a single electron transistor and sweep the gate voltage, we will be able to make an electron jump into or out of the island, changing the number of electrons on the island by one. So we will have no current whenever V_g is swept and get peaks in the current at specific V_g. The periodicity of the gate charge $Q_o=C_gV_g$ is equal to *e.* This effect is shown in Figure 21 (a) for sample 1 and 21 (b) for sample 2. A magnetic field of 0.1 T is applied to destroy the superconductivity in the island. The temperature is 50 mK and we apply a small bias voltage in the Coulomb Blockade region. For sample 1, the gate voltage where we get the peak in the current are -460mV, -205mV, 56 mV and 318 mV and for sample 2, -278 mV, -50 mV, 180 mV and 410mV. The coulomb blockade gap is minimum at these gate voltages. In the case of the normal state the coulomb blockade is zero and in the case of superconducting state, coulomb blockade gap is four times the superconducting gap ($4\Delta_o$).

From the gate voltage periodicity we get the gate capacitance of the samples using the Equation (19)

$$e = C_g (V_g - V_{g1}) \tag{19}$$

where V_g-V_{g1} is the difference between 2 consecutives gate voltage where we get the peak current.

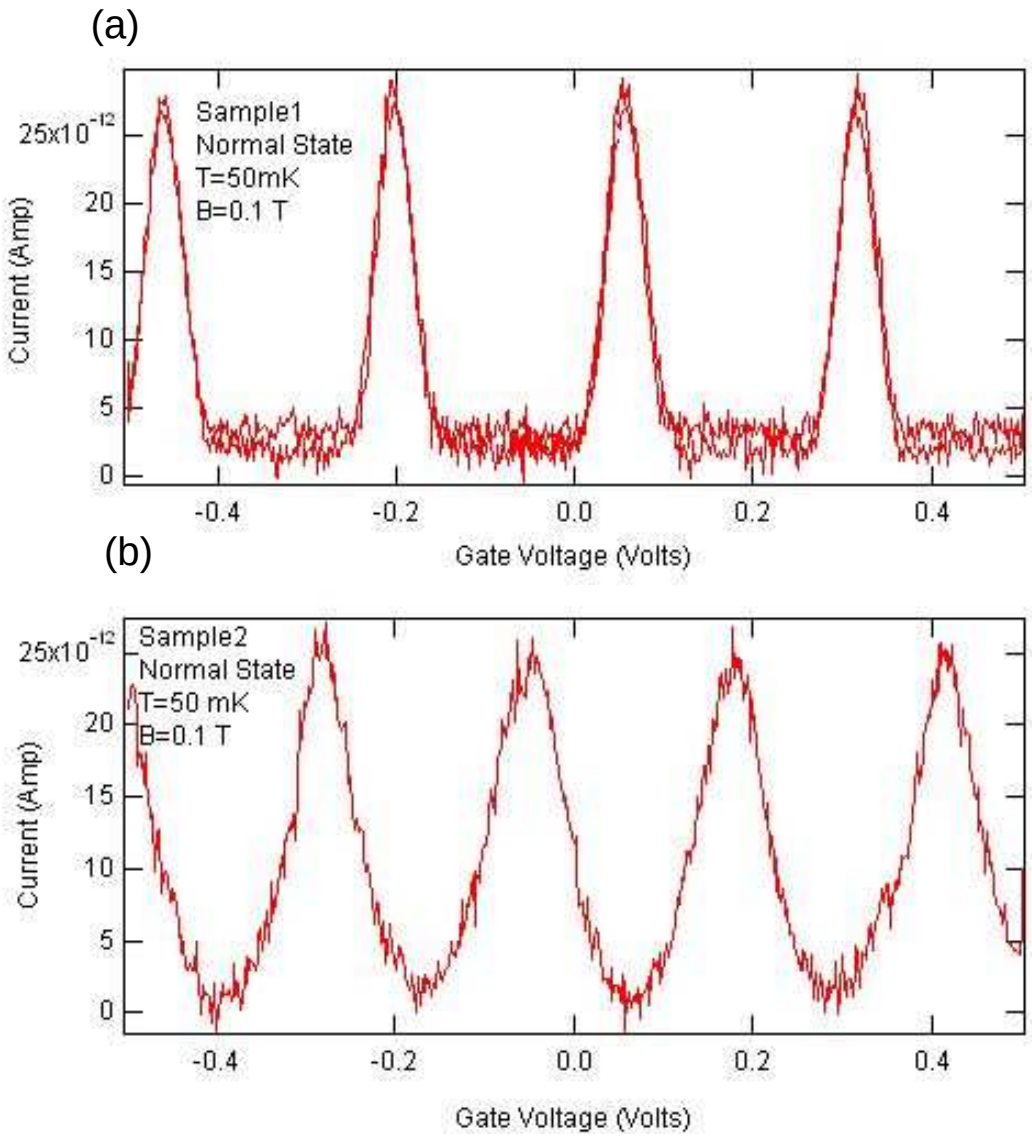

Figure 21. Low bias voltage I-Vg curves in the normal state at 50 mK (a) sample 1 (b) sample 2.

The gate capacitance of the samples are 0.55 aF for sample 1 and 0.71 aF for sample 2.

4.2. Charge Transport at High Bias.

The current in a SET starts increasing when the bias voltage is higher than the coulomb gap voltage (threshold voltage). As we can see from Figure 5 and Equations (11) and (12), the values of the thresholds are related to the capacitances of the junctions. To get the minimum bias voltage to start a current so that one electron jump from junction 1 into the island and then from the island to junction 2, we have to equalize Equation (11) to zero:

$$\Delta E_1^{\pm} = \frac{e^2}{C_\Sigma}\{[\frac{1}{2} \pm (n - \frac{Q_o}{e})] \pm \frac{C_2 V}{e}\} = 0 \qquad (20)$$

From Equation (20), we get.

$$V_{th,1}^{+} = \frac{-e}{C_2}\left[\frac{1}{2} + (n - \frac{Q_o}{e})\right] \qquad (21.a)$$

In the other case if we want the electron to jump from junction 2 into the island and then leave the island through junction 1, we equalize Equation (12) to zero and get

$$V_{th,2}^{-} = \frac{-e}{C_1}\left[\frac{1}{2} + (n - \frac{Q_o}{e})\right] \qquad (21.b)$$

If we work in the first rhombus area then n=0 and so on.

The only requirement that we accomplish is to get enough bias voltage to make an electron jump into the island because with that bias voltage, it is energetically favorable to make the electron jump out of the island through the other junction (Tinkham, 1996).

The Equations (21.a) and (21.b) are the line equations in Figure 5. Using both equations we get the capacitances in samples 1 and 2. For sample 1, C_1 = 42 aF and C_2 = 37 aF and for sample 2, C_1 = 45 aF and C_2 = 32 aF. Three IV curves for each sample are used to get these values.

Figure 22 shows the IV curves in the normal state at T=50 mK for our 2 samples. To break the superconductivity, an external magnetic field of 0.1 T is applied. The solid line is our data and the dashed line is the fitting curve that is obtained from the parameters indicated in the prior paragraph. We can observe that our data matches very well the fitting curve.

4.3. Periodicity of gate voltage.

As it was discussed in Section 4.1, the coulomb blockade gap is modulated with the gate voltage (dependence on the gate voltage) so we can increase or decrease the coulomb blockade gap while the gate voltage is swept. The minimum coulomb blockade is zero when the island is normal and is four times the superconducting gap when the island is a superconductor. These minimum coulomb blockade gaps are reached at the gate voltages found in Section 4.1.

Figure 23 shows the “coulomb diamonds” for sample 1 in the normal state. To destroy the superconductivity, an external magnetic field of 0.1 T is applied. The figure consists of several IV curves while the gate voltage is swept from -0.8 V to 0.8 V, letting us show several diamonds. The darker areas are where the coulomb blockade exists and there is no current at all.

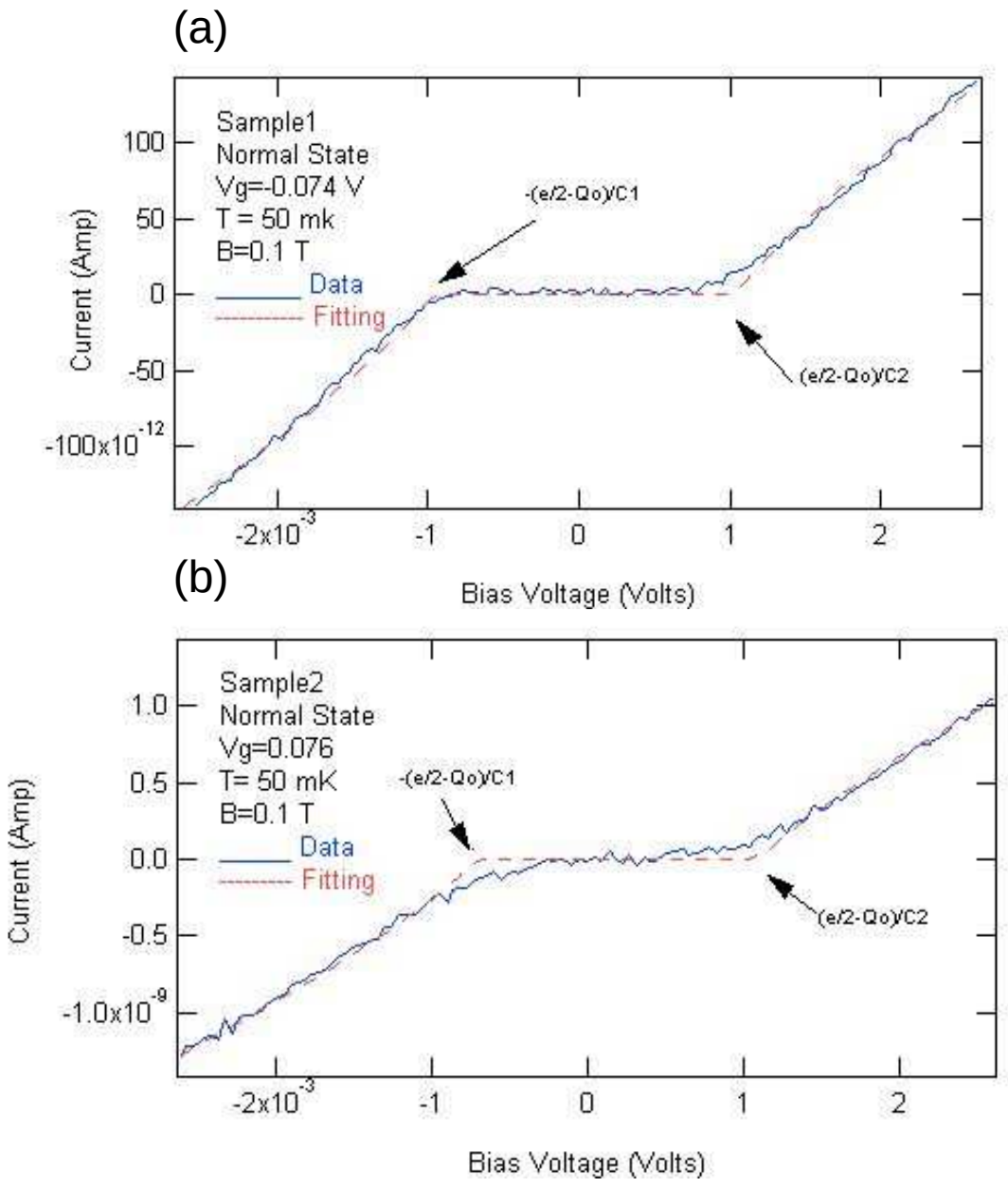

Figure 22. IV curves in the normal state at T=50 mK and B=0.1 T (a) sample 1 with Vg=74 mV (b) sample2 with Vg=76 mV

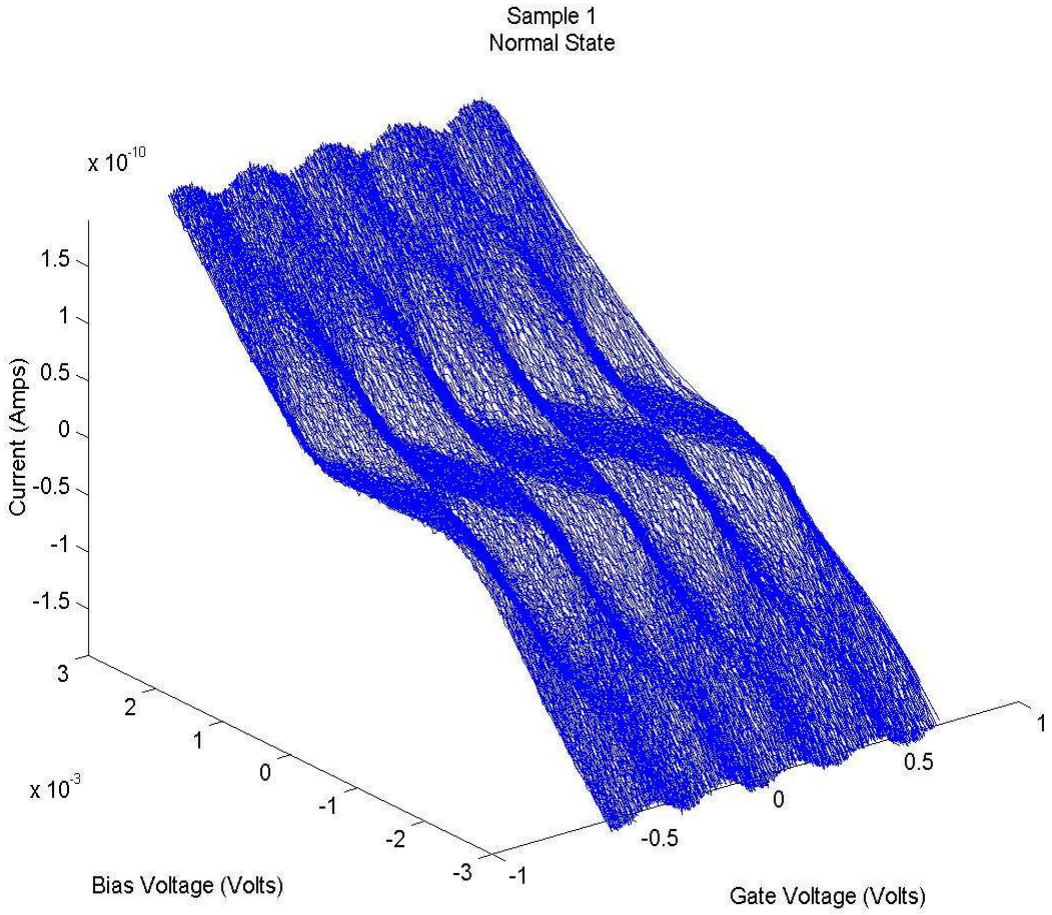

Figure 23. Experimental $I(V_g,V_b)$ surface for Sample 1 in the normal State at 50 mK. (B=0.1T). The minimum coulomb blockade voltage is equal to zero V_g is periodic.

These areas are rhombuses showing how the coulomb blockade gap increases and decreases as a periodic function of V_g. Because of the rhombic shape, these areas are known as “coulomb diamonds”.

The minimum coulomb blockade gap is zero because the island is in the normal state. The periodicity of gate voltage is approximately 0.285 eV.

Figure 24 shows the “coulomb diamonds” for sample 1 in the superconducting state at 50 mK. The figure consists of several IV curves while the gate voltage V_g is swept. The gate voltage is swept from -0.8 V to 0.8 V, letting us show several diamonds. The darker areas are where the coulomb blockade exists and there is no flow of electrons at all. The minimum threshold voltage is $2\Delta/e$ because it is the minimum supplied energy to create excitations in both junctions. So from this figure we get that the experimental superconducting gap is 226 μeV for sample1, It is observed that the coulomb blockade gap changes while we are sweeping the gate voltage showing the dependence between the coulomb blockade gap and the gate voltage.

Figure 25 shows the “coulomb diamonds” for sample 2 in the superconducting state at 50 mK. The figure consists of several IV curves while the gate voltage V_g is swept. The gate voltage is swept from -0.8 V to 0.8 V, letting us show several diamonds. The darker areas are where the coulomb blockade exists and there is not any flow of electrons. So from this figure we get that the experimental superconducting gap as 196 μeV for sample 2. The periodicity of gate voltage is approximately 0.229 eV. It is observed that the coulomb blockade gap changes while we are sweeping the gate voltage showing the dependence between the coulomb blockade gap and the gate voltage.

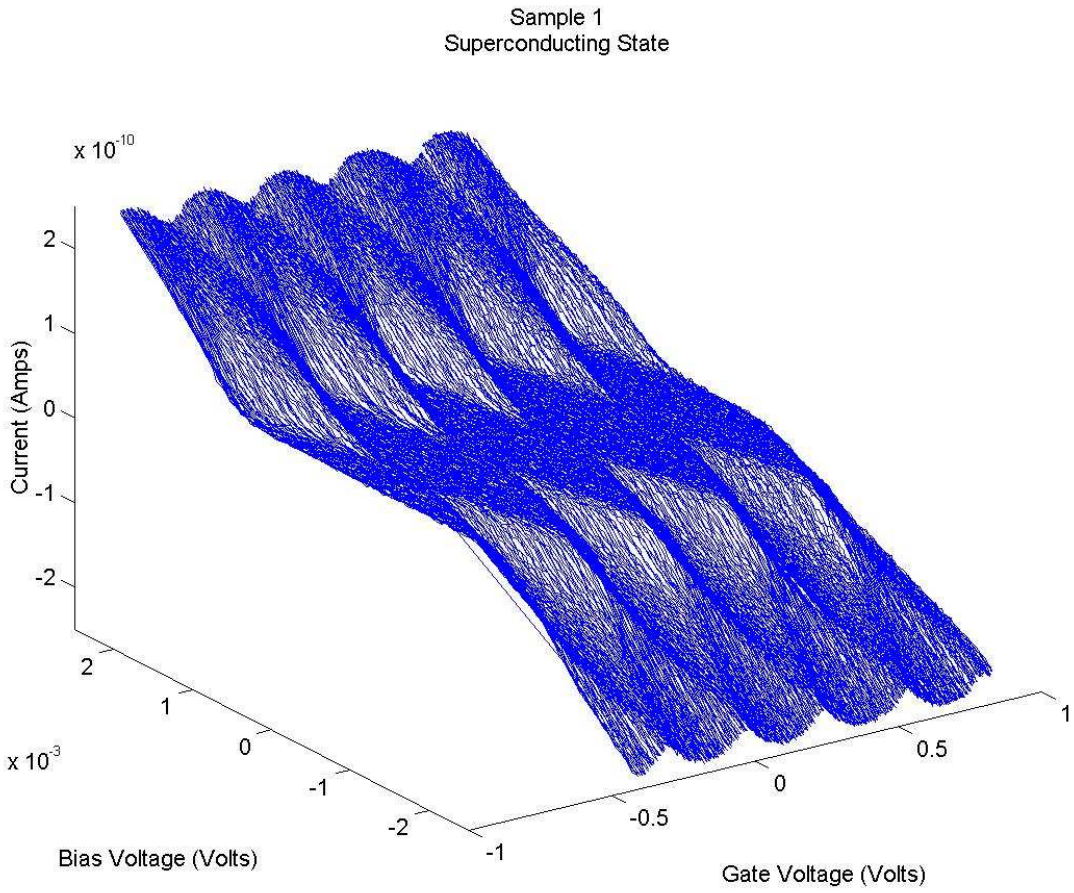

Figure 24. Experimental $I(V_g,V_b)$ surface for Sample 1 in the superconducting state at 50 mK. The minimum coulomb blockade voltage is equal to$2\Delta/e$ and V_g is periodic

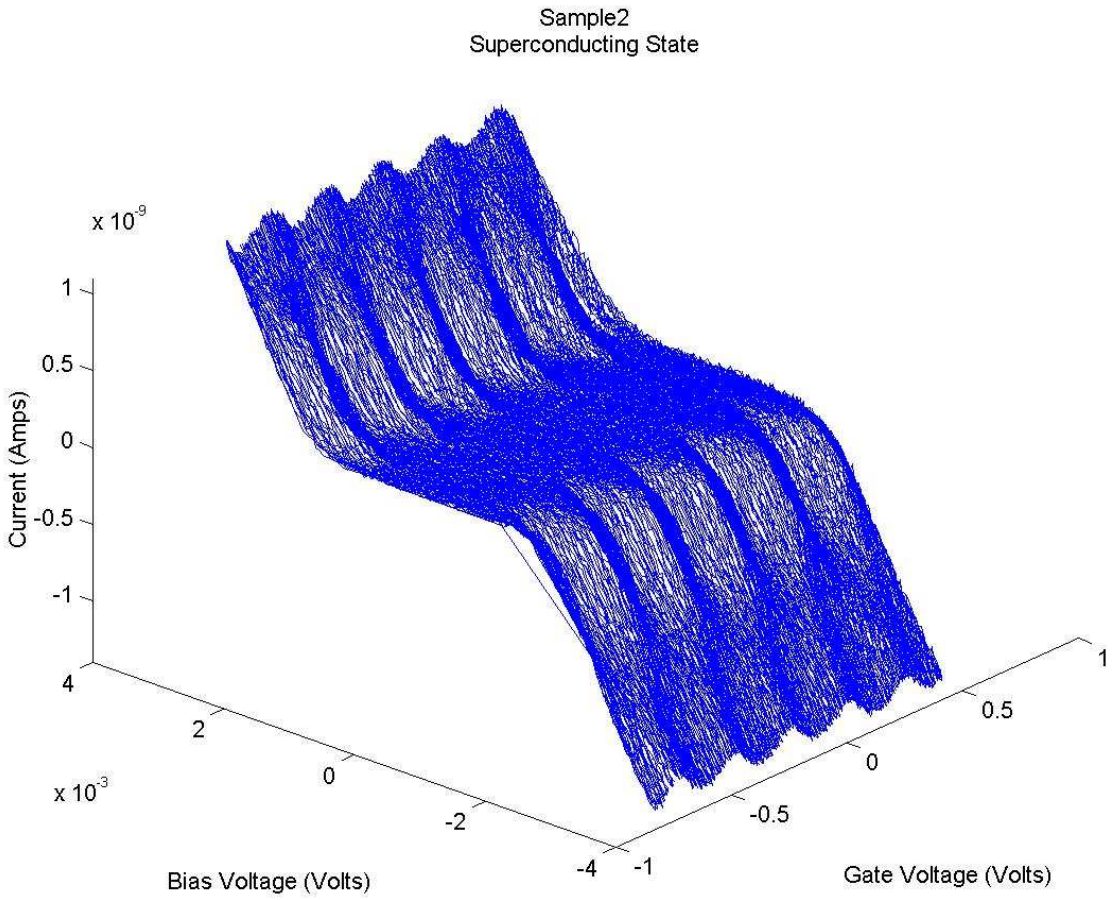

Figure 25. Experimental $I(V_g,V_b)$ surface for Sample 2 in the superconducting State at 50 mK. The minimum coulomb blockade voltage is equal to $2\Delta/e$ and V_g is periodic

4.4. Spin valve effect in the Normal state.

The goal of this test is to obtain the TMR in the normal state from the change of the current in the 2 different alignments of the source and drain and obtain the spin polarization P. With the spin polarization we can calculate approximately at which bias voltage we break the superconductivity completely in the island using the approximate relation $eV_c \sim \Delta_o P$. This relationship is valid in case that we have enough spin injection from our ferromagnetic leads and there is no any other effect.

We measure our samples in the normal state. To break the superconductivity, our samples are measured at 6K which is higher than the critical temperature of Aluminum (1.19 K). A constant bias voltage of approximately 4 mV is applied and an external magnetic field is swept from -0.1 T to 0.1 T forward and backward to have several scans. We take several scans to verify the correctness of the switching magnetic fields and besides get an average of the signal so the noise can be reduced.

Figure 26 shows the magneto resistance behavior of sample1 (a) and sample 2 (b) in the normal state at 6K. This data is the average over 20 scans; the average is done to reduce the noise in the signal. In sample 1, when the external magnetic field is swept from negative to positive, an increase in the resistance (decrease in the current) is observed, when the magnetization of source flips approximately at 24 mT, resulting in an antiparallel alignment between source and drain. When the magnetization of the drain flips at 35 mT, the magnetizations are parallel again, so a decrease in the resistance is observed. When the external magnetic field is swept from positive to negative, the spin valve effect is observed too, and in this case the switching magnetic fields are -24 mT and -35 mT.

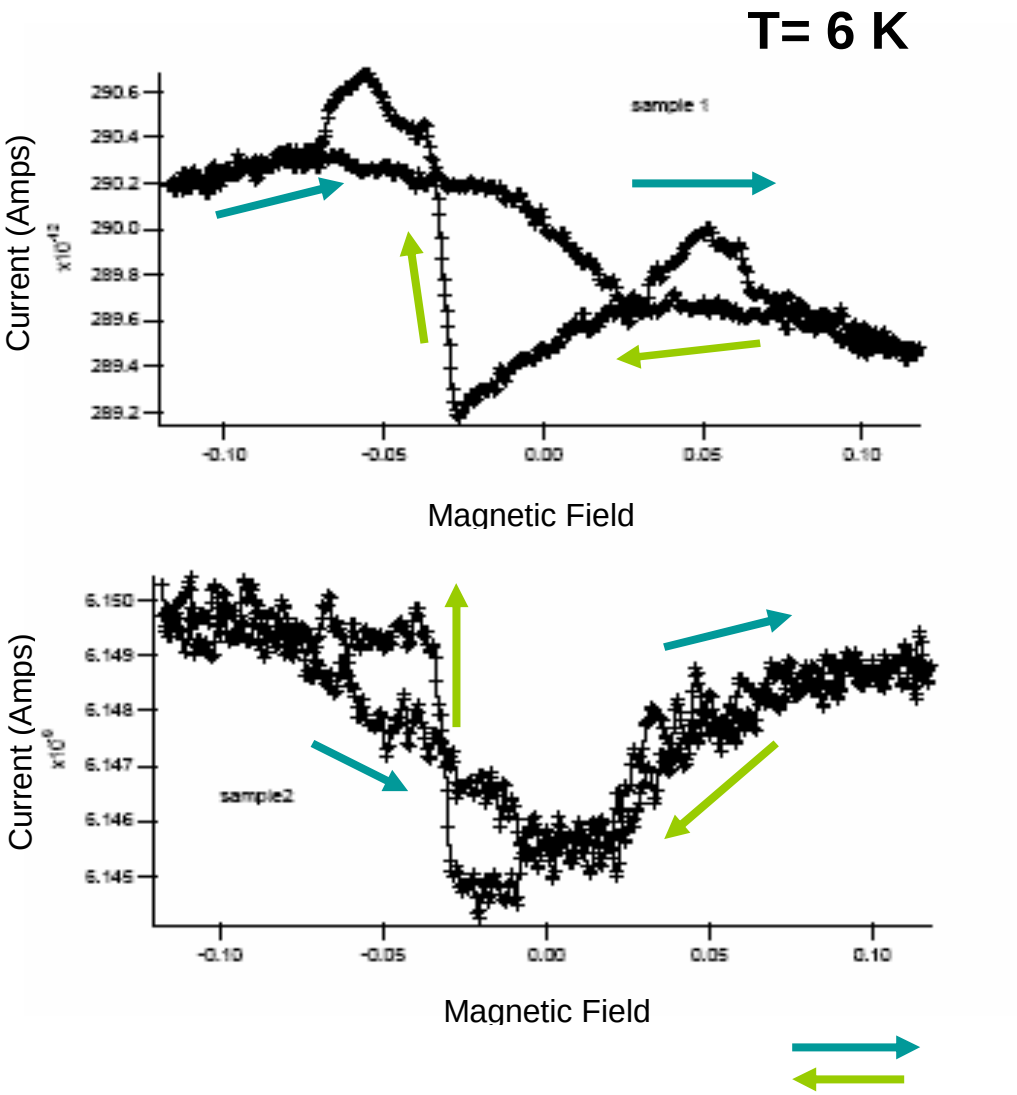

Figure 26. Spin valve effect at T=6 K for sample1 and sample 2 respectively. From the graph we can get the TMR's (0.48% and 0.08% for sample 1 and 2 respectively). The graphs were gotten after averaging 20 scans.

The hysteresis behavior is very similar to the hysteresis seen in previous works (Moodera, 1995). From the changes in the current, the TMR is calculated using Equation (13), getting a TMR equals to 0.48 %. Using Equation (15) and considering that the spin polarization in the drain is the same as the spin polarization of the source, we get a spin polarization of 5 %. In sample 2, when the external magnetic field is swept from negative to positive field, so that the magnetization of source flips approximately at 23 mT, an increase in the resistance (decrease in the current) is observed. When the magnetization of the drain flips at 37 mT, the magnetizations are parallel again so a decrease in the resistance is observed. When the external magnetic field is swept from positive to negative, the spin valve effect is observed too, and the switching magnetic fields are -23 mT and -37 mT. The TMR is 0.08 % and P is 2 %.

With these spin polarization the critical bias voltage to break superconductivity in the island completely for sample 2 is approximately 10 mV. As it was told before, this is only when there is enough spin polarization to produce the necessary spin accumulation in the island.

As we can observe, the spin injection efficiencies are very small in both samples. These small spin injection efficiencies can be due to the formation of random magnetic domains in our leads. The formation of random magnetic domains is due to 2 major reasons: one is the roughness of the surface and the other is that the antiparallel alignment is not favored in our actual geometry. This is why when one of the leads switches the direction of the magnetization some areas in the other lead tend to switch the direction of their magnetization because of their proximity among the edges (Johansson, 2003) as we can see in Figure 27 (Ashcroft, 1976).

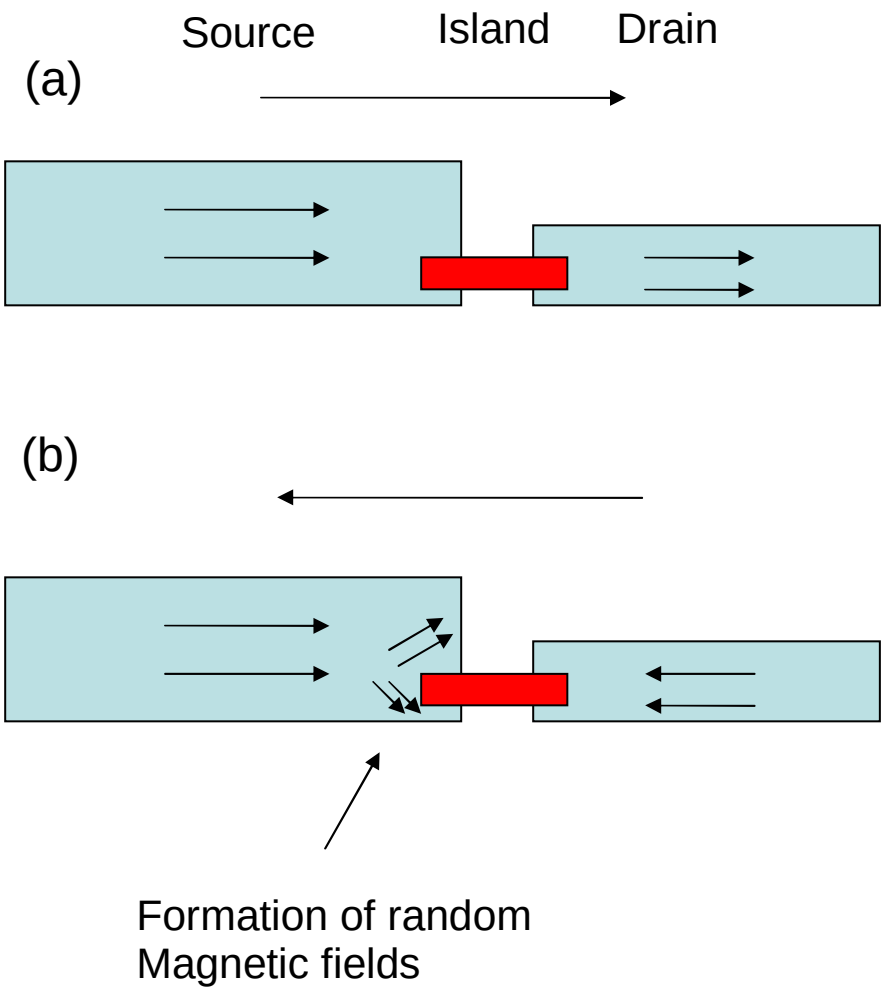

Figure 27. (a) Magnetic field in the parallel alignment (b) Formation of magnetic domains in the antiparallel alignment.

4.5. Suppression of Superconductivity.

The goals of this tests are to observe the magnetoresistance in the superconducting state while we are applying different bias voltage between source and drain so the effects that will be observed are the inverse magnetoresistance in a range right above the bias voltage where the superconducting gap starts decreasing and a suppression of the superconducting gap due to the fringing magnetic field of the ferromagnetic source and drain leads.

We measure our samples in the superconducting state at 50 mK, temperature that is lower than the critical temperature of Aluminum (1.19 K). The bias voltage is swept from 1 mV to 0 mV while an external magnetic field is swept from -0.1 T to 0.1 T forward and backward to have several scans. The sweeping frequency of the bias voltage is much lower than the sweeping frequency of the external magnetic field so we can get several current vs external magnetic field curves at “almost” constant bias voltage. The sweeping frequency of the bias voltage is 0.16 mHz and the sweeping frequency of the external magnetic field is 1.28 mHz. The gate voltage is zero.

Figure 28 shows several current vs the external magnetic field at different bias voltage for sample 2. For each current vs external magnetic field, the starting point in the current axis is a little shifted with respect of the ending point because the bias voltage is not completely constant. The right graph represents the current vs external magnetic field when the external magnetic field is swept from negative to positive magnetic fields (-0.1 T to 0.1 T) and the left graph represents the sweeping of the external magnetic field positive to negative (0.1T to -0.1T).

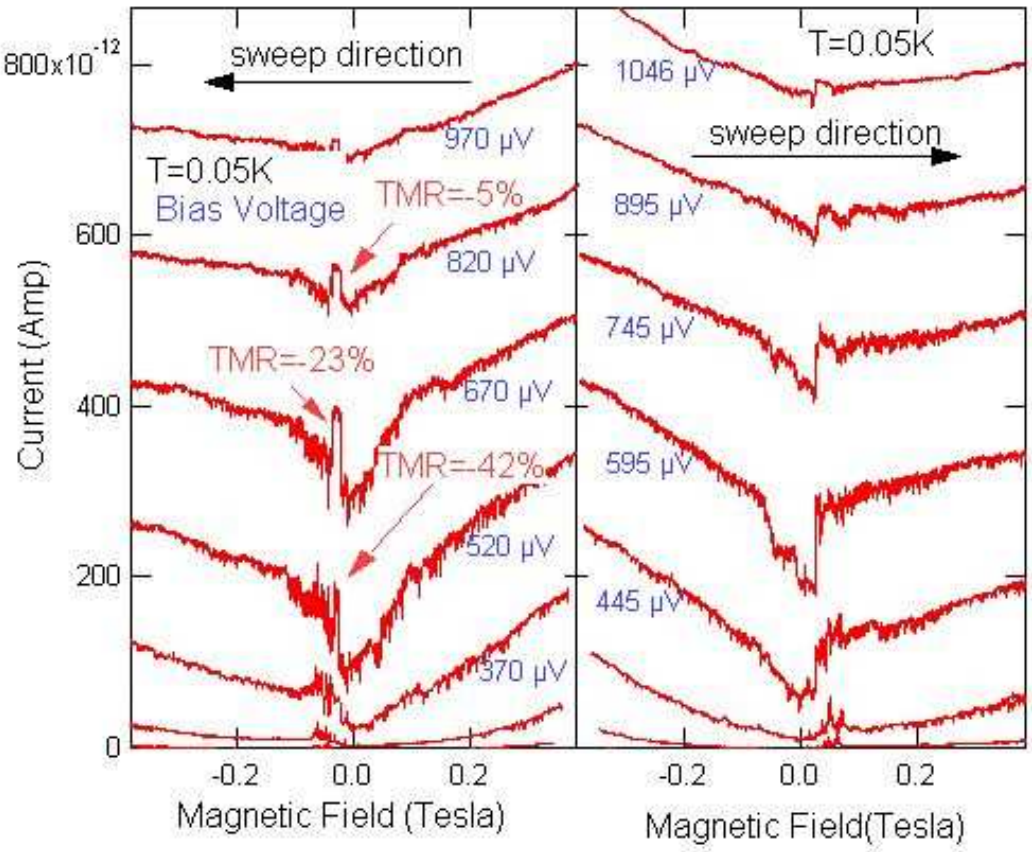

Figure 28. Current vs Magnetic field for different bias voltage. The left graph is when the sweep of the magnetic field is from positive to negative and the right graph is when the sweep is from negative to positive.

It is observed that when the sweeping of the external magnetic field is from positive to negative magnetic field, the current increases at -23 mT and decreases at -35 mT approximately and when the sweeping of the external magnetic field is from negative to positive, the current increases at 23 mT and decreases at 35 mT approximately. These are the same switching magnetic fields as those in the normal state so we can conclude that the alignment is antiparallel in these intervals. But the effect in the magneto resistance is completely different because what we observe is an inverse magnetoresistance so in the antiparallel alignment the current increases instead of decreasing like the normal state case. This inverse tunneling magneto resistance is obtained in the antiparallel alignment.

Another important effect besides the inverse magneto resistance that is showed is that absolute value of the change in the magneto resistance is greater than in normal state. While we get a TMR equal to 2% in the normal state, we can get a greater negative value of magneto resistance equal to -42% in the superconducting state.

The inverse magneto resistance is because the differential conductance in the antiparallel alignment increases faster than the differential conductance in the parallel alignment because of the decrease in the superconducting gap. The decrease of the superconducting gap is due to the fringing magnetic field produced by the source and drain leads because the decrease in the superconducting gap due to spin accumulation is expected at 10 mV, while we see suppressed gap at bias voltage below 1mV. The fringing magnetic field can certainly be strong enough to suppress the superconducting gap. As it was shown in Chapter 2, the peak of the fringing magnetic field that reaches the surface of the superconducting island is around 5000 Oe. This fringing magnetic field

suppresses the superconducting gap of the island considering that the critical magnetic field for Al is approximately 100 Oersted (Ashcroft, 1976).

Figure 29 shows 2 IV curves (positive voltage) for 2 different alignments. The solid line represents the IV curve for the antiparallel alignment and the dashed line represents the IV curve for the parallel alignment. To obtain this data, the frequency of the applied magnetic field is less than the frequency of the bias voltage so we obtain several IV curves for different magnetic fields. We require having at least half of the IV curve to be in range where the alignment is antiparallel. It is observed that the superconducting gap in the antiparallel alignment is less than the superconducting gap in the parallel alignment and this effect is what produces the inverse TMR observed in Figure 28.

In conclusion, the superconducting gap decreases due to the fringing magnetic field produced by the ferromagnetic leads and shows an inverse TMR because the superconducting gap decreases.

From the data, we observe that the superconducting gap is suppressed due to the fringing magnetic field produced by the ferromagnetic leads, but it does not completely vanish

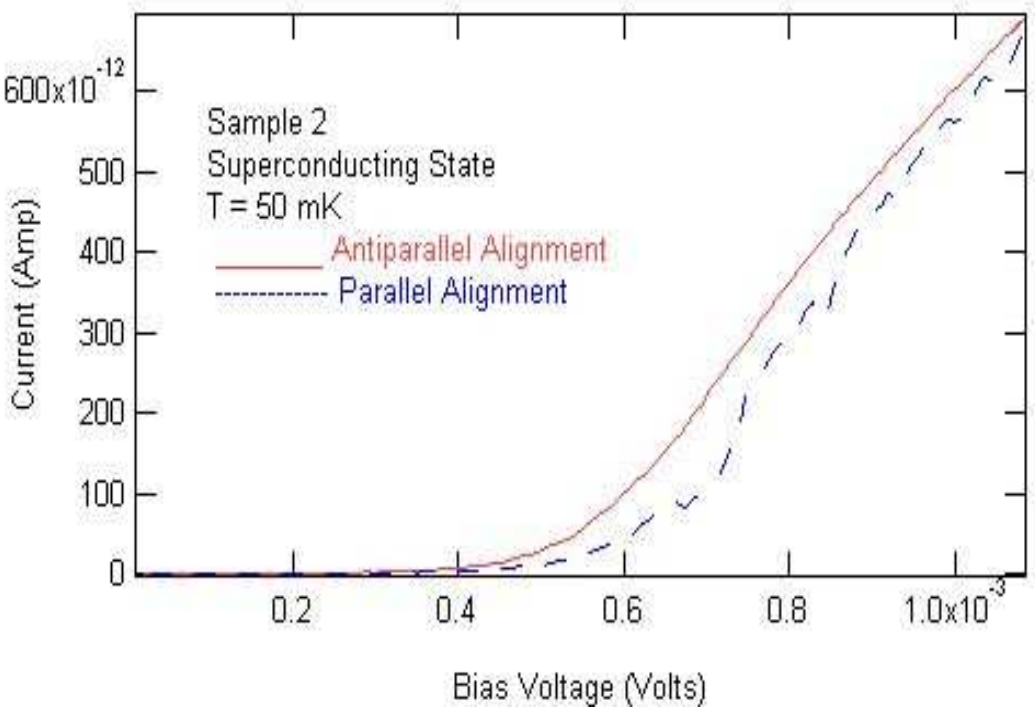

Figure 29. IV curves (positive quadrant) for sample 2 in the superconducting state (T=50mK). The solid line is in the antiparallel alignment and the dashed line is in the parallel alignment.

CHAPTER V

SUPPRESSION OF SUPERCONDUCTIVITY IN FERROMAGNET/SUPERCONDUCTOR/FERROMAGNET SINGLE ELECTRON TRANSISTOR DUE TO SPIN ACCUMULATION

According to Takahashi (Takahashi, 1999), if we have a SET with leads made of ferromagnetic metals and the island made of a superconducting metal, we will be able to suppress the superconductivity in the island due to the spin accumulation in the island while we are applying a bias voltage between source and drain.

To get this effect, we have to choose a proper geometry to minimize fringing magnetic field produced by ferromagnetic leads. The geometry used by us, was used previously by Chen (Chen, 2002), who claimed that the suppression of the superconductivity was due to the spin accumulation. As we can observe in our experiments, it is shown that the fringing magnetic field produced by the ferromagnetic leads is strong enough to suppress the superconductivity so this effect is dominant over the spin accumulation.

Another geometry that was used is what is proposed in Figure 30. In this geometry, the fringing magnetic field is minimized compared to the previous geometry, but one disadvantage is that the superconducting island is too close to the edges of the ferromagnetic leads and can still be affected by the fringing magnetic field. To reduce the effect of the fringing magnetic field, it is recommended to place the superconducting island at the center of the ferromagnetic leads, far from the edges.

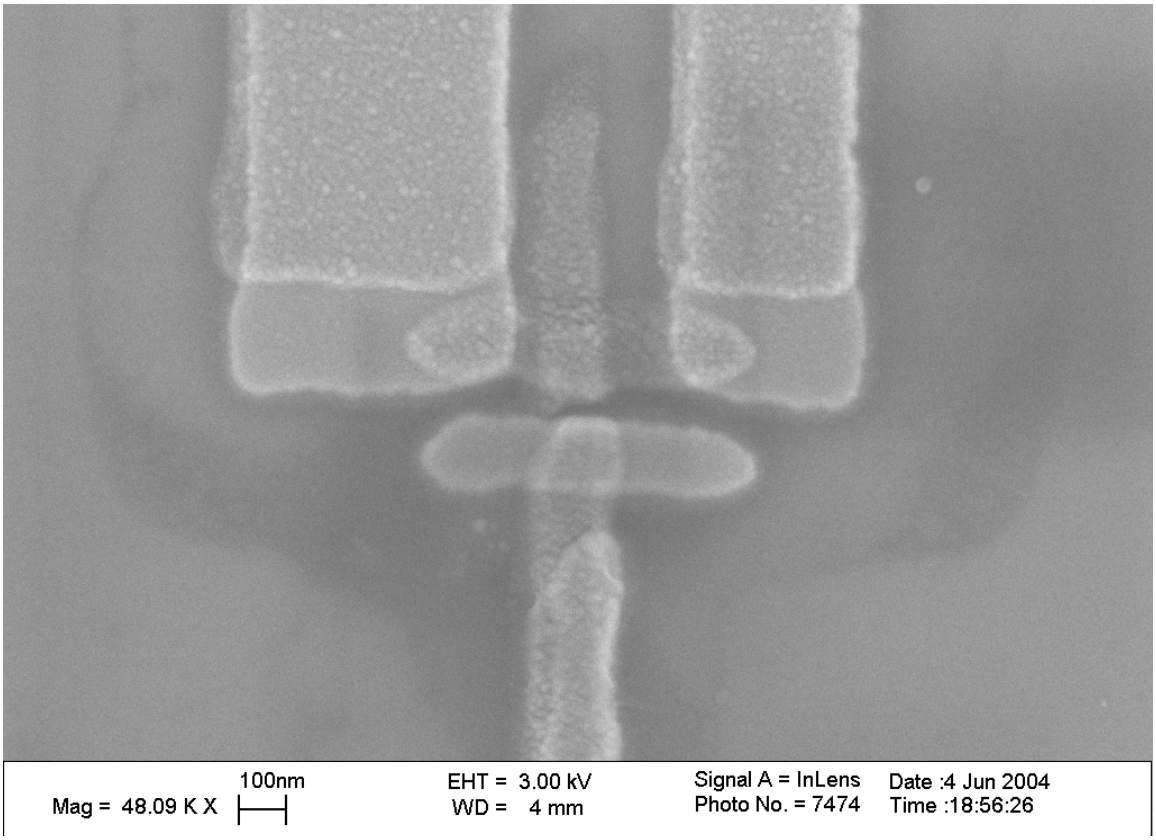

Figure 30. New geometry of FSF SET which minimizes the fringing magnetic field produced by the ferromagnetic leads and favors the antiparallel alignment.

The geometry shown in Figure 30 without the electrode probe at the middle of the superconducting island was used by Johansson (Johansson, 2003). In that paper, he claims that the suppression of the superconductivity obtained in his experiment is due to spin accumulation but the IV characteristics shown in the paper does not reflect the expected behavior of suppression of superconductivity due to spin accumulation. This expected qualitative behavior of the IV characteristics will be explained in the following paragraphs.

5.1. Expected qualitative behavior of the IV characteristics during the suppression of superconductivity of the island due to spin accumulation.

As it was explained in Chapter I, in 1976, Aronov explained theoretically the effects of the spin polarized current in superconducting metals (Aronov, 1976a). He predicted that a spin polarized current from the ferromagnetic metal would produce a nonequilibrium magnetization in the normal or superconducting metal so there would be a shift in the chemical potentials of the spin up and spin down electrons. In conclusion, to have spin accumulation, we need to have a spin polarized current flowing in the superconducting island of the FSF SET.

According to Takahashi (Takahashi, 1999), we will have spin accumulation in a FSF SET in the antiparallel alignment (considering that the junctions are symmetric), so we will be able to suppress the superconductivity in the island due to the spin accumulation. But we will start having spin accumulation in the island when the spin polarized current starts flowing so it is expected that the suppression of the superconductivity in the island will be at a bias voltage higher than the threshold voltage of the SET because there is no spin polarized current below threshold voltage.

When the superconductivity is suppressed, the current will jump to a value higher than the value of the current in the parallel alignment at the same bias voltage, so we will have a peak in TMR and this will be an inverse TMR because the current in the antiparallel alignment will be higher than that in the parallel alignment. This peak in the TMR will be at a bias voltage higher than the threshold voltage of the SET.

Comparing these conclusions with the results obtained by Johansson, we observe in Figure 31, that represents the IV characteristics obtained by Johansson, that the superconducting gap is suppressed in a bias voltage below the threshold voltage and a most pronounced spin-valve effect is obtained at a bias voltage ~ 200 μV, which is far below the threshold voltage where there is no spin polarized current, so it is not feasible to have spin accumulation.

In conclusion we disagree that the effect of suppression of the superconductivity obtained by Johansson is due to spin accumulation.

In Figure 32, we show qualitatively the behavior of the IV characteristics (positive quarter) of a FSF SET when the superconductivity in the island is suppressed due to the spin accumulation. The dashed line represents the IV curve in the parallel alignment and the solid line represents the antiparallel alignment. Below the threshold voltage there is no spin polarized current so the IV curves of parallel and antiparallel alignments have the same threshold voltage. When the bias voltage is higher than the threshold voltage, there will be spin polarized current and spin accumulation will appear in the island in the antiparallel alignment as predicted by Takahashi.

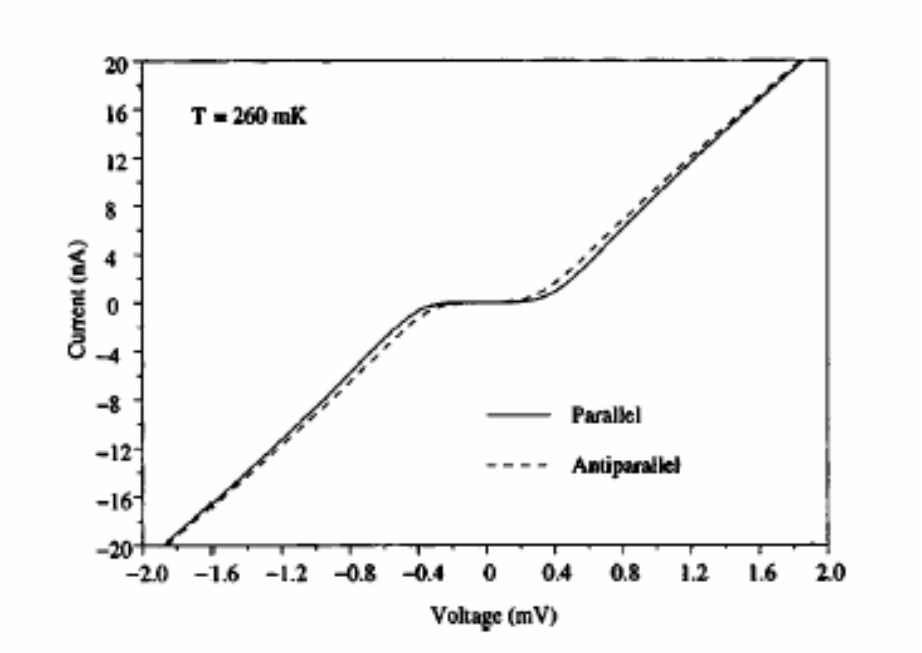

Figure 31. (Johansson, 2003) IV characteristics of a Co/Al/Co double tunnel junction, in the stable parallel (P) and the antiparallel (AP) state of the Co electrodes.

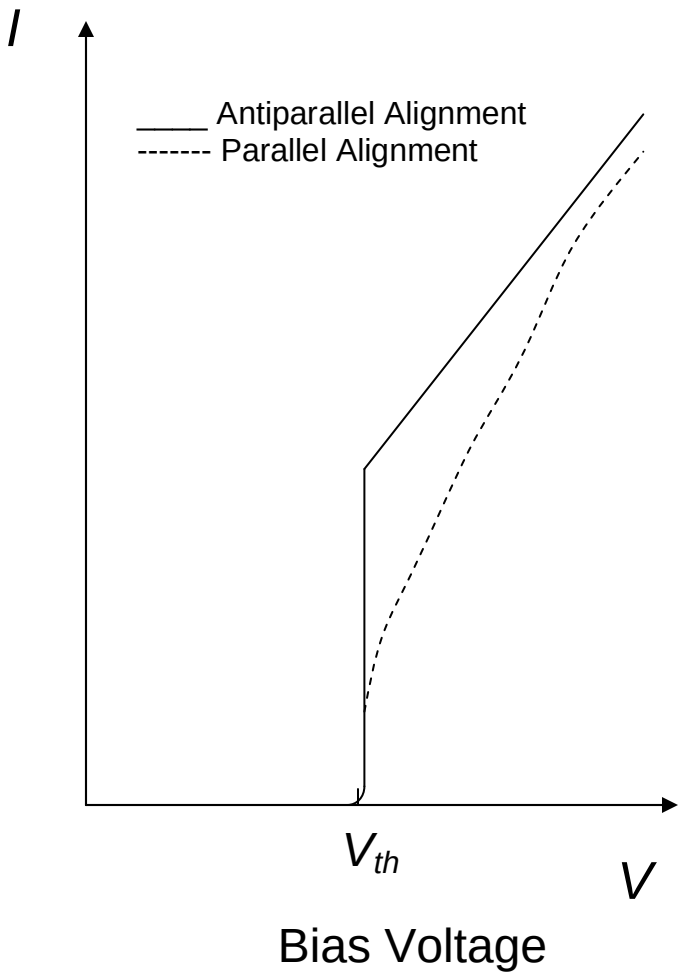

Figure 32. Qualitatively IV characterisitics (positive quarter) for a FSF SET in the parallel and the antiparallel alignment

At a certain bias voltage above the threshold voltage, the superconductivity is suppressed by the spin imbalance. The spin accumulation produces a shift in the chemical potentials of both quasiparticles (spin up and spin down). Then this shift in the chemical potentials plays the role of pair breaking energy. During the suppression of the superconductivity due to spin accumulation, the current in the antiparallel alignment jumps to a higher value than the current in the parallel alignment so there will be an enhancement of the TMR and the effect will be an inverse TMR.

The bias voltage where the superconductivity is suppressed is known as the critical bias voltage and it is inversely proportional to the spin polarization (Takahashi, 1999).

CHAPTER V

CONCLUSIONS

Small single electron transistors were fabricated using a state of the art e-beam lithography and shadow evaporation technique. The size of the device was below 200 nm.

The small SET's showed a spinvalve effect in the normal state of the island.

It is shown that the superconducting gap in the superconducting island in the SET decreases due to the strong fringing magnetic field produced by the magnetization of source and drain leads. According to our calculations, the fringing magnetic field produced by one of the ferromagnetic leads is approximately 5000 Oe, strong enough to suppress the superconducting gap in the island. This is an additional method of controlling superconductivity.

An inverse TMR for some range of bias voltage is observed. This is produced because the differential conductance in the antiparallel alignment depends not only on the bias voltage but also on the decrease of the superconducting gap so the differential conductance in the antiparallel alignment increases faster than the differential conductance in the parallel alignment. This magnetoresistive effect is new because all the effects that were studied before consist in positive TMR.

It is observed that our spin injection is low. This could be caused by several reasons but one that is very important it is the formation of random magnetic domains in the leads

due to our geometry that makes the antiparallel alignment unfavorable. Also the roughness of the surface was another reason.

The suppression of the superconducting gap in the island is not due to the spin accumulation but the fringing magnetic field produce by the ferromagnetic leads. We conclude this because the spin polarization is low so the spin accumulation is not enough to shift the chemical potentials of the majority and minority quasiparticles in the superconducting island.

The TMR in our samples were 0.48% and 0.1% in the normal state. The depression of the TMR effect in general is caused predominantly by spin relaxation effect in the island and the spin polarization. We consider that the cause of the low TMR is the spin polarization that was discussed in the paragraph above. We do not consider that the spin relaxation is a predominant reason of the low TMR because our contact resistances are in the range where we can neglect the spin relaxation. As it was explained in Chapter 2, the time between 2 consecutive tunneling effects should be less than the spin relaxation time ($\tau_s > \tau_t$). Using this condition, we have, for Al, τ_s ~ 10^{-10} sec (Jedema, 2002) at 4.2 K, in our case we work at 50 mK so τ_s is longer (Fabian, 1999 and Yamashita, 2002).

$\tau_t = dD_N e^2 R_c A$ (Heslinga, 1993) where d is the thickness of the superconducting layer (in our case d~200 Å), D_N is density of states (for Al 10^{22}/(eV cm^3)), A is the contact area, R_c is the tunnel resistance. So

$\tau_s > \tau_t$

$10^{-10} > dD_N e^2 R_c A$

Using the values we got in the paragraph above and considering a contact area of 1500 $Å^2$, we got that $R_c < 250$ KΩ. Our contact resistances are in this range.

For future projects to observe a suppression of the superconducting gap due to the spin accumulation in the island, it is recommended to change the geometry of the FSF SET so that we can obtain 2 improvements:

- The antiparallel alignment is favorable and the parallel alignment can be controlled by the external magnetic field.
- The fringing magnetic field produced by the ferromagnetic leads can be minimized.

A geometry that produces these 2 improvements is shown in Figure 30.

APPENDIX A

PUBLISHED PAPERS

A. Anaya, R. Bhaumik, D. Davidovic, “Suppression of superconductivity due to fringing magnetic field in Ferromagnet-Superconductor-Ferromagnet Single Electron Transistor”, To submit to Journal of Applied Physics.

A. Anaya, M. Bowman and D. Davidovic, “Suppression of spin-orbit scattering in Strongly Disordered Gold Nanofunctions.“, Phys Rev Letter 93,246604 (2004)

M.Bowman, A.Anaya, A.L.Korotkov and D.Davidovic, “Localization and capacitance fluctuations in disordered Nanojunctions.“, Phys. Rev. B 69, 205405 (2004).

A.Anaya, A.L.Korotkov, M.Bowman,J.Waddell and D.Davidovic, “Nanometer-scale grains connected with atomic-scale conductors.”, Journal of Applied Physics, 93,3501 (2003)

D.Davidovic, A.Anaya, A.L.Korotkov, M.Bowman and M.Tinkham, “Electron Transport in Metallic Grains”, Journal of The Physical Society of Japan, Vol.72, Suppl. A. pp106-111 (2003)

REFERENCES

Aronov, A. G., (1976a), ‘‘Spin injection and polarization of excitations and nuclei in superconductors’’, Zh. Eksp. Teor. Fiz. 71, 370–376 [Sov. Phys. JETP 44, 193–196 (1976)].

Aronov, A. G., (1976b), ‘‘Spin injection in metals and polarization of nuclei’’, Pis’ma Zh. Eksp. Teor. Fiz. 24, 37–39 [JETP Lett. 24, 32–34 (1976)].

Ashcroft, N. and D. Mermin, (1976), “Solid State Physics”, Brooks Cole, 1976

Averin, D.V. and K.K. Likharev, (1991), “Mesoscopic Phenomena in Solids”, Elsevier Science Publishers B.V. 1991.

Baibich, M. N., J. M. Broto, A. Fert, F. Nguyen Van Dau, F. Petroff, P. Eitenne, G. Creuzet, A. Friederich, and J. Chazelas, (1988), ‘‘Giant magnetoresistance of (001)Fe/(001)Cr magnetic superlattices’’ , Phys. Rev. Lett. 61, 2472–2475.

C.D. Chen, W. Kuo, D.S. Chung, J.H. Shyu, and C.S. Wu. (2002), “Evidence for Suppression of Superconductivity by Spin Imbalance in Co-Al-Co Single-Electron Transistor”, Phys. Rev. Lett. 88,047004 (2002)

Clinton, T.W., and Mark Johnson (1997), “Mesoscopic magnetoquenched Superconducting valve”, Appl. Phys. Lett. 70, 1170 (1997).

Clinton, T.W., and Mark Johnson (1999), “Nonvolatile switchable Josephson Junctions”, Journal of Applied Physics. 85, 1637 (1999).

Clinton, T.W., and Mark Johnson (2000), “Magnetoquenched superconducting valve with bilayer ferromagnetic film for uniaxial switching”, Appl. Phys. Lett. 76, 2116 (2000).

Devoret, Michel H., Esteve, Daniel, and Urbina, Christian (1992), "Single-electron Transfer in Metallic Nanostructures", *Nature*, Vol. 360, 10 December 1992, pp. 547-553.

Dong, Z.W. et al. (1997), ‘‘Spin-polarized quasiparticle injection devices using Au/YBa2Cu3O7 /LaAlO3 / Nd0.7Sr0.3MnO3 heterostructures’’, Appl. Phys. Lett. 71, 1718 (1997).

Dolan, G.J. (1977), “Offset masks for lift-off lithography”, Applied Phys. Lett 31, 337

Fabian, J. & Das Sarma (1999), “S. Phonon-induced spin relaxation of conduction electrons in aluminium”, Phys. Rev. Lett. 83, 1211–1214

Fulton, T.A. and G.J. Dolan (1987), “Observation of Single-Electron Charging Effects in Small Tunnel Junctions”, Phys. Rev. Lett. 59, 109

Giaever, I. and H.R. Zeller (1968), “Superconductivity of Small Tin Particles Measured by Tunneling”, Phys. Rev. Lett. 20, 1504

Heslinga D.R. and T.M. Klapwijk (1993), “Enhancement of Superconductivity far above the critical temperature in double-barrier tunnel junctions”, Phys. Rev. B 47, 5157

Jedema, F.J.; H.B. Heersche, A.T. Filip, J.J.A. Baselmans, B.J. van Wees, (2002), “Electrical detection of spin precession in a metallic mesoscopic spin valve”, Nature 416, 713

Jin, S., T.H. Tiefel, M. McCormack, R.A. Fastnacht, R. Ramesh, and L.H.Chen (1994), “Thousanfold Change in Resistivity in Magnetoresistive La-Ca-Mn-O Films”, Science, 264, 413-415

J. Johansson, M. Urech, D. B. Haviland, and V. Korenivski (2003), Comment on "Evidence for Suppression of Superconductivity by Spin Imbalance in Co-Al-Co Single-Electron Transistors", Phys. Rev. Lett. 91, 149701

Johansson, J., Mattias Urech, David Haviland, and V. Korenivski (2003), “Suppression of Superconductivity due to Spin Imbalance in Co/Al/Co single electron transistor”, Journal of Applied Physics, 93, 8650

Johnson, Mark, and Robert H. Silsbee (1985), “Interfacial charge-spin coupling: Injection and detection of spin magnetization in metals”, Phys. Rev. Lett. 55, 1790 – 1793.

Johnson, Mark , (1994), “Spin coupled resistance observed in ferromagnet-superconductor-ferromagnet trilayers”, Appl. Phys. Lett. 65, 1460

Julliere, M., (1975), ‘‘Tunneling between ferromagnetic films’’ , Phys. Lett. A 54, 225 – 226.

J. S. Moodera, L. R. Kinder, T. M. Wong, and R. Meservey, (1995), “Large Magnetoresistance at room temperature in Ferromagnetic Thin Films Tunnel Junctions”, Phys. Rev. Lett. 55, 3273–3276.

Mott, N. F., (1936a), “The electrical conductivity of transition metals”, Proc. R. Soc. London, Ser. A 153, 699–717.

Sarma, G., J. (1963), “On the influence of a uniform exchange field acting on the spins of the conduction electrons in a superconductor”, Phys. Chem. Solids 24, 1029

Takahashi, S., H. Imamura, and S. Maekawa. (1999), “Spin Imbalance and Magnetoresistance in Ferromagnet/Superconductor/Ferromagnet Double Tunnel Junctions”, Phys. Rev. Lett. 82, 3911.

Takahashi, S., H. Imamura, and S. Maekawa. (2000), “Spin Injection and magnetoresistance in ferromagnet-superconductor-ferromagnet tunnel junctions”, Journal of Applied Phys., 87, 5227.

Tedrow, Paul M., and Robert Meservey (1970), “Magnetic Field Splitting of the Quasiparticle States in Superconducting Aluminum Films”, Phys. Rev. Lett. 25, 1270–1272.

Tedrow, Paul M., and Robert Meservey (1971), “Spin-dependent tunneling into ferromagnetic Nickel”, Phys. Rev. Lett. 26, 192–195.

Tedrow, P. M., and R. Meservey (1973), “Spin polarization of electrons tunneling from films of Fe, Co, Ni, Gd”, Phys. Rev.B 7, 318–326.

M. Tinkham, (1972), “Tunneling Generation, Relaxation and Tunneling Detection of Hole-Electron Imbalance in Superconductors”, Phys. Rev. B 6, 1747

M. Tinkham, (1996), “Introduction to Superconductivity” , McGraw-Hill, New York, 1996

Vas’ko, V.A. , V. A. Larkin, P. A. Kraus, K. R. Nikolaev, D. E. Grupp, C. A. Nordman, and A. M. Goldman (1997), ‘‘Critical current suppression in a semiconductor by injection of spin polarized carriers from a ferromagnet,’’, Phys. Rev. Lett. 78, 1134

Yamashita, Takahashi, Immamura and Maekawa (2002), “Spin Transport and relaxation in superconductors”, Phys. Rev. B 65, 172509

Wolf, S.A.; Awschalom, D.D, R.A. Buhrman, J.M. Daughton, S. Von Molnar, M.L. Roukes, A. Y. Chtchelkanova, D.M. Treger (2001), “Spintronics: A Spin-Based Electronics Vision for the Future”, Science, Vol. 294 Issue 5546, p1488